Offprints from:
Prigogine-Rice: Advances in Chemical Physics, Vol. 40
John Wiley & Sons, Inc.

DYNAMICS OF CRYSTAL GROWTH

JOHN D. WEEKS AND GEORGE H. GILMER

Bell Laboratories
Murray Hill, New Jersey 07974

CONTENTS

I. Introduction 157
II. The Kinetic SOS Model 159
III. Simple Theories for the Dynamics of Crystal Growth 164
A. Exact Kinetic Equations 164
B. Approximate Evaluation of the Evaporation Rate 167
1. Wilson-Frenkel Theory 167
2. Temkin Mean Field Theory 168
3. Two Rate Model 169
IV. Nucleation Theory of Crystal Growth 177
A. Classical Theory of Heterogeneous Nucleation 177
B. Atomistic Nucleation Theory 182
C. Interface Motion by 2d Nucleation 184
V. The Surface at Equilibrium and the Roughening Transition 190
VI. Dynamics of the Roughening Transition 197
VII. Spiral Growth and the Influence of Line Defects 204
A. Screw Dislocations 204
B. Asymmetry Between Crystal Growth and Evaporation 213
VIII. Impurities 217
A. Impurity-Enhanced Nucleation 217
B. Segregation of Impurities During Crystal Growth 219
IX. Final Remarks 224

I. INTRODUCTION

In this article we discuss from a microscopic point of view theories for the transfer of material from a fluid to a crystalline phase. We emphasize the processes occurring in the interfacial region, where the atoms or molecules from the fluid assume the ordered arrangement of the crystal lattice. Our purpose is to evaluate the different factors that affect crystal growth, including the structure of the interface, impurities, defects in the crystal lattice, and the mobility of atoms at the interface. Morphological stability of the crystal[1] and other aspects of crystal growth associated with bulk transport are not discussed.

Recent progress in understanding fundamental aspects of interface kinetics has come primarily from studies of a kinetic Ising (or lattice gas) model[2] of the crystal-vapor interface. This model gives an atomic-scale representation of the growing crystal, including the atomic processes of condensation, evaporation, and surface migration, and can describe the structure of different crystal faces as well as the effects of lattice imperfections such as screw dislocations and impurities.[3–6] The kinetic Ising model has a relatively simple mathematical description and yet it is capable of treating all the above phenomena which are known to have important influences on the crystal growth kinetics. Thus it provides a convenient starting point for further theoretical analysis and is also well suited for computer simulation "experiments." Monte Carlo (MC) simulations can provide an arbitrarily accurate treatment of the model with all the complexities mentioned above, limited only by the amount of computer time available, whereas the theoretical methods are usually applied to more idealized situations.

Using this model, we describe several recent theoretical advances that have been made in our understanding of both the static (equilibrium) and dynamic (growth) behavior of low-index impurity-free faces of a perfect crystal. The computer simulations are also reviewed. These results provide an important test of the accuracy of the analytic methods in their regime of applicability and indicate the changes that arise in more complicated situations.

Section II gives a brief mathematical description of the model for the simplest case of the (001) solid-vapor interface of a perfect impurity free simple cubic (SC) crystal. Some limitations inherent in the model are pointed out. In Section III we review several simple theories of crystal growth for this case. These theories are derived from an exact kinetic equation which describes the impingement, evaporation, and surface migration of atoms on the crystal surface. However, the surface structure is treated by mean field approximations. These methods prove most accurate at high temperatures or high impingement rates where continuous (nonnucleated) growth occurs. At low temperatures and for small driving forces, crystal growth must proceed by a nucleation mechanism. Section IV contains a discussion of a version of the classical nucleation theory of Becker and Doering[7] applied to nucleation on a crystal surface. This serves as a basis for the development of a more detailed atomistic nucleation theory. Both approaches are compared to a MC simulation specifically designed to test the ideas of nucleation theory. The growth rates of low index faces are then related to the nucleation and spreading of clusters at the crystal surface.

None of these theories adequately describes the transition region from nucleated to continuous growth. In Section V we discuss the change in the equilibrium structure of the crystal-vapor interface that occurs at the *roughening temperature* T_R. Below T_R the surface is basically flat with only small clusters of adatoms or surface vacancies present, whereas above T_R arbitrarily large clusters can be found and the interface extends over many lattice planes. It is this change in the structure of the interface that then allows for different modes of growth above and below T_R. The static properties of the roughening transition are analyzed and related to phase transitions in several other model systems.

In Section VI dynamic properties of the roughening transition are analyzed using methods that have been successfully applied to study dynamic critical phenomena. A renormalization group analysis relates the change in growth rates above and below T_R to the changes in equilibrium correlations between different parts of the interface that occur at the roughening temperature.

In Section VII we discuss the relation of linear defects in the crystal lattice to crystal growth rates. The classical theory of spiral growth about screw dislocations is briefly reviewed and compared with recent MC calculations. For an understanding of the more complex situations where both spiral growth and two-dimensional (2d) nucleation occur, we rely mainly on the MC results. We also compare the kinetics of growth with that of evaporation and suggest reasons for the asymmetry observed in experimental data. Monte Carlo data on a crystal containing a small columnar hole exhibits a similar asymmetry.

In Section VIII we consider two aspects crystal growth in the presence of impurities: (1) impurity enhancement of 2d nucleation growth kinetics and (2) the trapping of weakly bonded impurities at the surface of a growing crystal. Again, most of the quantitative results are obtained by simulation. Final comments and conclusions are found in Section IX.

II. THE KINETIC SOS MODEL

We consider here the simple case of a (001) solid-vapor interface of an impurity-free SC crystal. More general situations can be easily described. Consider the ordinary lattice gas (Ising model) in which each site in a SC lattice is either vacant or occupied by a single atom whose interaction energy with another atom in a nearest neighbor site is ϕ. Longer-ranged interactions are ignored. If we further require that every occupied site be directly above another occupied site (thus excluding "overhangs") we obtain the *solid-on-solid* (SOS) model.[4] The SOS system can be equally well described as an array of interacting columns of varying integer heights. The surface configuration is represented by a square array of

integers which specifies the number of atoms in each column perpendicular to the (001) plane, that is, the height of each column. Growth or evaporation of the crystal involves the "surface atoms" at the tops of their columns.

This SOS model is a generalization of the familiar terrace-ledge-kink model[8] in the sense that it permits clusters of adatoms, surface vacancies, and irregular step structures (see Fig. 1). [Note that the addition or removal of an atom from a *kink site* (denoted K in Fig. 1) leaves another kink site present. These repeatable step sites play an important role in the theory of crystal growth.] The SOS model is a special case of the lattice gas model, since it is required that each atom have another one directly below it, that is, overhangs are excluded. At low temperatures the SOS model is an accurate approximation to the lattice gas because the surface remains quite flat and overhangs are energetically unfavorable. The SOS model is simpler to study than the usual lattice gas model because a 2d array of height variables is required to specify a configuration rather than the 3d array of occupation numbers needed for the lattice gas.

The energy of a particular configuration (i.e., a particular choice of the set of heights $\{h_i\}$ for all the columns in the system) is determined by

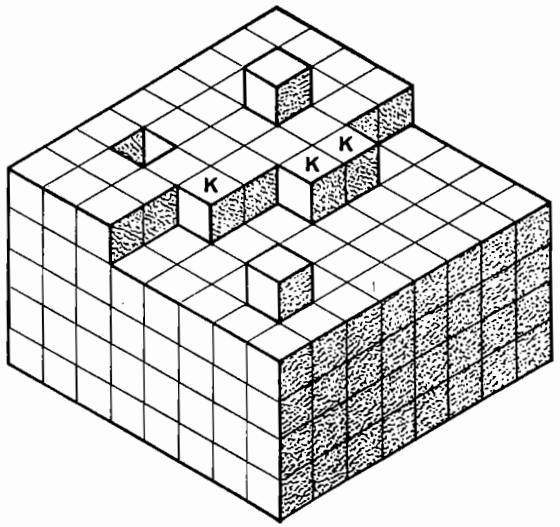

Fig. 1. Atoms on a (001) face of a SC crystal. Surface atoms may have up to four lateral neighbors. An atom in a kink site, indicated by a K in the figure, has two lateral neighbors.

counting the number of nearest neighbor bonds. Thus

$$E_{SOS}(\{h_i\}) = E_0 - \frac{\phi}{2}\sum_{j,\delta} \min(h_j, h_{j+\delta}) - \phi\sum_j h_j \tag{2.1}$$

Here E_0 is the energy of the crystal when $h_i = 0$ for all columns of atoms. The second term on the right-hand side accounts for the lateral bonds; the number of such bonds between column j and one of its nearest neighbors at $j+\delta$ is equal to the smaller of the numbers h_j and $h_{j+\delta}$. The summation in j includes all columns, and δ includes all nearest neighbors of column j. The factor of $\frac{1}{2}$ corrects for double counting. The third term accounts for the vertical bonds within a given column.

The equilibrium properties of an open system are determined by the grand canonical partition function. This is a summation over all sets $\{h_i\}$, that is,

$$\Xi = \sum_{\{h_i\}} \exp[-\beta E_{SOS}(\{h_i\}) + \beta\mu N(\{h_i\})] \tag{2.2}$$

where

$$N(\{h_i\}) = N_0 + \sum_j h_j \tag{2.3}$$

N_0 is the number of atoms in the configuration with all $h_i = 0$ and $\beta = (kT)^{-1}$ with T the absolute temperature and k Boltzmann's constant. (Throughout this article references to low or high temperatures imply values of the dimensionless temperature kT/ϕ much less than or greater than unity.) The value of the chemical potential for two-phase equilibrium is $\mu = \mu_{eq} = -3\phi$.[9] If we insert this in (2.2) and replace E and N using (2.1) and (2.3), we obtain

$$\Xi = \exp(-\beta E_0 + \beta\mu_{eq}N_0)\sum_{\{h_i\}} \exp[-(\beta J/2)\sum_{j,\delta} |h_j - h_{j+\delta}|] \tag{2.4}$$

Here $J \equiv \phi/2$, and we have made use of the identity

$$|h_j - h_{j+\delta}| = h_j + h_{j+\delta} - 2\min(h_j, h_{j+\delta}) \tag{2.5}$$

The partition function in (2.4) contains only differences between the height variables h_j and $h_{j+\delta}$. Configurations that differ by a vertical translation of an integral number of lattice spacings have identical probabilities. This is consistent with equilibrium between the vapor and crystal phases and confirms the value of the chemical potential $\mu_{eq} = -3\phi$.

Equation 2.4 can be obtained directly in the case of the equivalent spin system in zero field. The energy of the lateral pairs of overturned spins is

(neglecting an additive constant)

$$E_{\text{Ising}} = \frac{J}{2} \sum_{j,\delta} |h_j - h_{j+\delta}| \tag{2.6}$$

The total number of spins is fixed, and the canonical partition function is equivalent to (2.4). For simplicity, we often refer to the expression in (2.6) as the energy of the SOS system, although it includes chemical potential terms when the lattice gas interpretation is used.

Although no one has been able to evaluate (2.4) exactly using analytic methods, much progress has been made recently by studying related models with slightly different interaction energies.[10-12] The MC method has also been used to obtain very accurate thermodynamic and structural data for this system.[9,13,14] This work is reviewed in Section V.

Dynamics is introduced into the model by creating or annihilating atoms at random positions on the surface. This simulates the molecular exchange between the solid and vapor phases. The rate of creation (deposition) of atoms per site at the surface, denoted k^+, is assumed to be independent of the neighboring surface configurations. Physically we are envisioning the random impingement and attachment of atoms from the vapor phase. The deposition rate is proportional to the pressure in a pure vapor system, and in general we write

$$k^+ = k_{eq} \exp(\beta \Delta\mu) \tag{2.7}$$

where $\Delta\mu$ is the deviation of the chemical potential from its equilibrium value and k_{eq} is the deposition rate at equilibrium. Its value is calculated in Section III.

Although it is reasonable to assume that the deposition rate is independent of the neighboring surface configurations, the annihilation (evaporation) rate of a surface atom depends very critically on the number of nearest-neighbor bonds that must be broken in the evaporation process. We assume here that the evaporation rate of an atom with m lateral neighbors ($0 \leq m \leq 4$ in a cubic lattice) is

$$k_m = \nu e^{-m\beta\phi} \tag{2.8}$$

where ν is the evaporation rate of an isolated adatom at the surface. Thus the more neighbors an atom has, the slower is its evaporation rate. Note the very strong temperature dependence of the evaporation rate caused by the activated process of breaking bonds. The net evaporation rate, and hence the total growth rate of the crystal, depends on the detailed structure, in particular, the amount of clustering found at the interface.

Another important process in the kinetics of crystal growth is surface migration or diffusion, in which a surface atom hops from one site to an unoccupied site on the surface. Generally the rate of migration is greater than that for evaporation, since the migrating atoms may remain within the region of the attractive surface interactions. Radioactive tracer methods and measurements on the relaxation of perturbations in the structure of metal-vapor interfaces have demonstrated the importance of mass transport along the surface.[15] It is easy to see that the qualitative effect of surface diffusion is to increase the growth rate, since atoms which impinge on sites with few bonds to the crystal can jump to more favorable positions and hence are less likely to evaporate. For simplicity in the mathematical formalism that follows, we consider a restricted form of surface migration in which a surface atom on a given layer can hop only to unoccupied sites in the *same* layer. Generally this is the most important process. This restriction is not needed in the MC simulations.

The above picture models most directly growth from the vapor phase of materials with short-ranged intermolecular forces, for example vapor-deposited growth of semiconductor crystals. Other kinetic models with different impingement and evaporation probabilities may be more appropriate for melt and solution growth cases. (The energy parameter ϕ must of course also be chosen differently for these cases.) However, the equilibrium structure of the interface and (as shown in Section V) many features of the dynamic behavior of the system near the roughening transition are independent of the kinetics assumed. In what follows, we concentrate on the simple vapor growth case.

We emphasize that the above represents a probabilistic *model* for the dynamics of crystal growth. An exact description of the incorporation of atoms from the vapor into the crystal lattice would involve the solution of Newton's equations of motion for the system. The impingement from the vapor, the loss of the initial kinetic energy, and the final attachment to the lattice are idealized in our model, as is the description of the evaporation process. However, the model does give a consistent and physically reasonable description of the cooperative interactions among clusters of atoms that are crucial to the crystal growth process. A more fundamental treatment based on Newton's equations seems at present prohibitively difficult.

In comparing our results to those of real systems, one must keep in mind the limitations of the model we use. For example, the lattice structure must be chosen *a priori*, and hence this model cannot be used to investigate the formation of dislocations or extended lattice defects. However, if a lattice containing defects is specified initially, their effect on the kinetics can be measured. The assumption that atoms occupy sites in a

perfect lattice is also an oversimplification. However, recent work reviewed in Sections V and VI suggests that this restriction is not important in studies of the roughening transition.

In all our discussions we assume that it is possible to achieve equilibrium conditions where the crystalline and fluid phases coexist with one another. If the temperature is below the triple point temperature, the disordered phase is the vapor, whereas it is a dense fluid above the triple point. The energy parameter ϕ must be changed to try to describe these two very different situations. The SOS model itself gives no indication of where this change should occur or what its magnitude should be. When the temperature is increased still further, it is often very difficult in the laboratory to achieve pressures large enough to maintain two-phase equilibrium and prevent the crystal from melting. Thus at high temperatures the model may describe an experimentally unrealizable situation. Further, the no-overhang restriction of the SOS model becomes increasingly unrealistic at very high temperatures. Hence the high temperature limit of the model may not be applicable to the more common crystalline materials. The predictions of the model are most realistic at low and moderate temperatures, and it is in this regime that we concentrate our efforts in the sections that follow. Properly interpreted, the kinetic SOS model provides a useful compromise between mathematical simplicity and physical reality. In this article we hope to demonstrate its utility as a versatile model of the crystal growth process.

III. SIMPLE THEORIES FOR THE DYNAMICS OF CRYSTAL GROWTH

In this section we use the kinetic SOS model to derive several simple theories for the dynamics of crystal growth. We are mainly interested in calculating the crystal growth rate as a function of the imposed driving force and the temperature for the simple case of growth on a (001) face of a SC crystal that is free of impurities and dislocations. Crystal growth in more complicated situations is discussed in Sections VII and VIII.

We first write down a set of kinetic equations which in principle provide an exact description of growth in the kinetic SOS model.[16] Although an exact solution of these equations is not possible, some approximate solutions based on mean field theory are easy to find. These prove most accurate at high temperatures and high deposition rates and provide a starting point for further developments in the continuous growth regime.

A. Exact Kinetic Equations

Let $C_n(t)$ be the fraction of sites in the nth layer parallel to some (001) reference plane which is occupied by atoms at time t. Because of the exclusion of overhangs, the fraction of surface atoms in the nth layer (i.e., atoms at the tops of their columns with the site directly above unoccupied) is given by

$$P_n = C_n - C_{n+1} \tag{3.1}$$

In other words, P_n is the probability of finding a particular column whose height extends to layer n. We suppress the argument t when no confusion will result.

By definition,

$$C_n = \sum_{k=n}^{\infty} P_k \qquad \sum_{n=-\infty}^{\infty} P_n = 1 \tag{3.2}$$

Finally, let $P_{n;m}$ be the probability that a surface atom in the nth layer has m lateral neighbors ($0 \leq m \leq 4$). Clearly,

$$P_n = \sum_{m=0}^{4} P_{n;m} \tag{3.3}$$

Then $f_{n;m}$, the fraction of surface atoms in the nth layer with m lateral neighbors (bonds), is given by

$$f_{n;m} \equiv P_{n;m}/P_n \tag{3.4}$$

It is easy to write an exact equation for the kinetic SOS model describing the rate of change of the $C_n(t)$ using (3.1) to (3.4) along with (2.8):

$$\frac{dC_n(t)}{dt} = k^+[C_{n-1}(t) - C_n(t)] - \nu \sum_{m=0}^{4} e^{-m\beta\phi} P_{n;m}(t) \tag{3.5}$$

$$= k^+ P_{n-1}(t) - k(n,t) P_n(t), \tag{3.6a}$$

$$= k^+[C_{n-1}(t) - C_n(t)] - k(n,t)[C_n(t) - C_{n+1}(t)] \tag{3.6b}$$

Here:

$$k(n,t) = \nu \sum_{m=0}^{4} e^{-m\beta\phi} f_{n;m}(t) \tag{3.7}$$

represents the *effective evaporation rate* of surface atoms in layer n at time t.

The first term on the right in (3.5) is the product of the deposition rate k^+ with the fraction of sites in layer n that are available for deposition, that is sites that are occupied in layer $n-1$ but not already occupied in layer n. The second term gives the rate at which surface atoms in layer n evaporate; this depends on the number of nearest neighbors of each atom as determined by the $P_{n;m}$ functions.

The total crystal growth rate R is the difference between the rate of

deposition in all layers R^+ and the rate of evaporation from all the layers R^-:

$$R = R^+ - R^- \tag{3.8}$$

where, using (3.5) to (3.7),

$$R^+ = k^+ \sum_{n=-\infty}^{\infty} P_{n-1} = k^+ \tag{3.9}$$

and

$$R^- = \sum_{n=-\infty}^{\infty} k(n,t) P_n \tag{3.10}$$

Equation 3.5 is not a closed equation for the $C_n(t)$, since it also involves the more complicated functions $P_{n;m}(t)$ or equivalently $f_{n;m}(t)$. These functions describe the amount of clustering present during growth and hence contain the essential physics of the growth process. The amount of clustering varies dramatically with temperature and deposition rate (see Fig. 2). Rather, (3.5) is the first member of a hierarchy of equations relating lower-order distribution functions to higher-order functions.

Note in particular that with our restricted version of surface diffusion (no change in surface level on diffusion) all effects of surface diffusion are contained implicitly in the $f_{n;m}$ functions. Surface diffusion increases the growth rate by increasing the fraction of atoms having many neighbors (i.e., atoms in a cluster) which consequently are much less likely to evaporate.

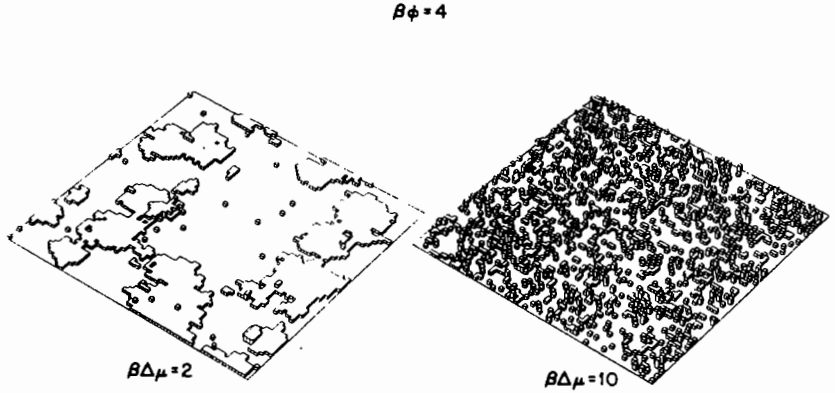

Fig. 2. Typical MC interface configurations after deposition of 25% of a monolayer on a flat (001) face of the crystal. The temperature is identical for the two cases, but $\beta\Delta\mu = 2$ for the interface on the left and $\beta\Delta\mu = 10$ on the right.

As rewritten in (3.6), all these complications are hidden in the definition of the effective evaporation rate $k(n,t)$ in (3.7). We discuss several theories of crystal growth which make some approximations based on physical intuition or mathematical convenience as to the form of the $k(n,t)$. These closures implicitly describe the amount of clustering present and allow (3.6) to be solved to give approximations to the growth profile $C_n(t)$ and the growth rate R. This basic approach is most accurate at high temperatures or high driving force where the amount of clustering can be estimated using the assumption of a random distribution of adatoms. At very low temperatures and low driving force, the more explicit cluster formation picture of classical nucleation theory is required. This is reviewed in Section IV together with recent work which puts the theory on a more fundamental basis and tests by MC simulations many of its assumptions. At higher temperatures approaching the roughening temperature, the nucleation picture breaks down. A theory describing dynamics near the roughening transition is given in Section VI.

B. Approximate Evaluation of the Evaporation Rate

1. *Wilson-Frenkel Theory*

The simplest possible assumption about the evaporation rate during growth is to assert that it is the same as that from a surface at equilibrium. This equilibrium rate can be easily calculated. A layer can, in principle, grow (or be removed) by successive creations (annihilations) of atoms only at kink sites (see Fig. 1). The *equilibrium* deposition rate $k^+_{eq} \equiv k_{eq}$ must then equal the kink site evaporation rate $\nu e^{-2\beta\phi}$. Further, this must equal the total equilibrium evaporation rate R^-_{eq} if the growth rate R in (3.8) is to be zero. Thus

$$R^-_{eq} = k_{eq} = \nu e^{-2\beta\phi} \tag{3.11}$$

The simple *Wilson-Frenkel* expression[17] for the growth rate is then, using (3.8) and (2.7),

$$R_{WF} = k^+ - R^-_{eq} = k_{eq}(e^{\beta\Delta\mu} - 1) \tag{3.12}$$

Equation 3.12 in general greatly overestimates the growth rate, since it assumes the maximum possible (equilibrium) clustering at the surface. Thus it represents an upper bound to the actual growth rate. It should be accurate at very high temperatures when essentially all atoms evaporate at the same rate and perhaps also in the case of very rapid surface diffusion. However, there is no indication of where it can be trusted and where it might fail. For small enough $\Delta\mu$, the WF growth rate is linearly proportional to the driving force (i.e., linear growth is predicted), so (3.12) fails completely in the nucleation regime.

2. *Temkin Mean Field Theory*

More ambitious approaches make use of the detailed equations of motion, (3.5) to (3.7). For this method to be useful, one must first assume a form for the effective evaporation rate $k(n, t)$. The Temkin mean field theory[18] approximates $k(n, t)$ as the evaporation rate of an atom with a "typical" number of nearest neighbors. In our model an atom with m neighbors has an evaporation rate $\nu e^{-m\beta\phi}$ [see (2.8)]. The Temkin theory asserts

$$k^T(n, t) = \nu e^{-\langle m\rangle_n \beta\phi} \tag{3.13}$$

where $\langle m\rangle_n$ is the average number of neighbors of an atom in layer n. This in turn is approximated by the average number of neighbors in a *random distribution* of the atoms. If the probability of finding an atom at a given site in the nth layer is C_n, then $4C_n$ gives the average occupancy of the four nearest-neighbor sites in a random distribution. Thus the Temkin approximation for $k(n, t)$ is

$$k^T(n, t) = \nu e^{-4\beta\phi C_n(t)} \tag{3.14}$$

The Temkin approximation for $k(n, t)$ depends only on the average occupancy of a layer, as is characteristic of mean field approaches. Such an expression would in fact be exact for a system with infinitely long-ranged and infinitely weak forces in the lateral directions. Every atom then interacts equally with every other atom in that layer and has an evaporation rate determined by the average occupancy as given in (3.14). This limit is an artificial one, far removed from the nearest-neighbor interactions originally assumed.

Furthermore, since clustering has no effect on the energy or evaporation rate of the atoms, growth cannot proceed by a nucleation mechanism. As a result, the mean field equations always give a region of "metastable states" where the predicted growth rate is rigorously zero, although there is a finite driving force applied to the system. These metastable states are artifacts of the mean field approximation. In fact, because nucleation can occur (even if it is very improbable), there will always be some growth in response to a finite driving force, even well below the roughening temperature. The critical value of the driving force required to produce growth in mean field theory is much greater than that found by the MC calculations. (In the latter case there is always some growth in response to a finite driving force, but we can define a region where the growth rate is negligibly small.) Thus mean field theory does not give even a qualitatively accurate description of growth below T_R.

Above T_R the width of the metastable state regime becomes very much smaller (but never disappears entirely), and mean field theory offers a quantitatively accurate theory over a rather wide range of nonzero driving forces. It also correctly describes the approach at very high temperatures to the Wilson-Frenkel limiting growth law.

Strictly speaking, however, because there are metastable states even above T_R, the mean field theory fails to provide the limiting linear growth law that should result from the application of a very small (infinitesimal) driving force. It is also incapable of describing the effect of surface diffusion on the growth rate. Since surface diffusion does not change the average layer concentration in our model, the mean field expression, (3.14), predicts the same growth rate for a system with and without surface diffusion. This must be looked on as a rather serious failing of the mean field approach.

Figure 3 compares the numerical integration of (3.6) using the mean field expression, (3.14), with the MC results (with no surface diffusion allowed) at a temperature just above T_R. Note that the mean field results exhibit a small metastable state region, whereas the MC calculations show linear growth for small $\Delta\mu$. Aside from this region, the two curves are in good agreement. The results become even better at higher temperatures. At lower temperatures the metastable state region greatly increases in width and the mean field theory is very inaccurate.

3. *Two Rate Model*

Next we review a simple and completely analytic theory of crystal growth introduced by Weeks, Gilmer, and Jackson[16] that does predict a

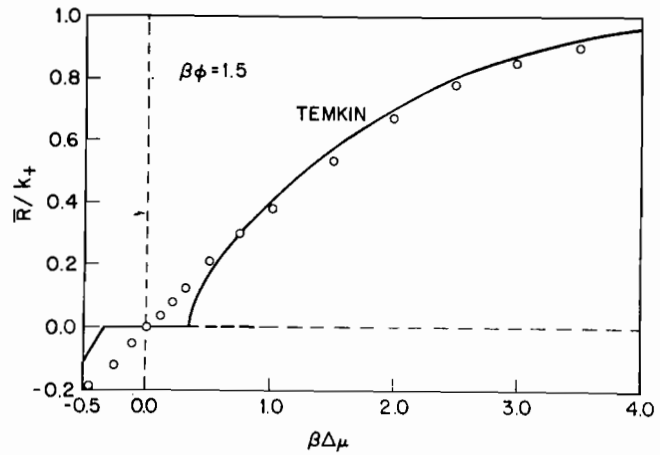

Fig. 3. Comparison of growth rates calculated by the MC method, circles, and the Temkin mean field model, solid line. The Temkin model has metastable states in the region $-0.33 < \beta\Delta\mu < 0.33$. Here $\beta\phi = 1.5$.

linear growth rate at small driving force. Provided a single empirical parameter is chosen properly, the theory gives results in quantitative agreement with MC calculations above T_R. Unfortunately, this approach also gives linear growth below T_R, but the predicted growth rate is very small and so differs little in magnitude from the correct value. The qualitative effects of surface diffusion can also be understood in this approach. A reader primarily interested in the results of this method could skip the derivation that follows and begin with (3.43).

We begin the analysis by making several simplifications and approximations in the basic equations, (3.5) to (3.7). One simplification is to study only the steady-state solution. After an initial transient period (typically after a few layers have grown), MC simulations have shown that the average growth rate $\bar{R}$ reaches a steady-state value (see Section IV). It is reasonable to suppose that when this occurs, the structure of a given layer n at time t can be related to that of layer $n-1$ at time $t-\tau$, where τ is the time required to deposit a monolayer of material on the surface. Thus we expect

$$C_n(t) = C_{n-1}(t-\tau) = C_{n+1}(t+\tau) \tag{3.15}$$

and

$$k(n,\tau) = k(n-1, t-\tau) = k(n+1, t+\tau) \tag{3.16}$$

Here we assume that at steady-state growth, the state of each successive layer repeats the conditions of the preceding layer at an earlier time. [Note from (3.7) that for (3.16) to hold we must assume the $f_{n;m}$ repeat themselves in the same manner.]

Strictly speaking, for a crystal of infinite cross-sectional area which is observed over an infinite period of time, this very plausible assumption is incorrect. Because of fluctuations in the growth condition of widely separated regions of a given layer (e.g., variations in the rate of formation and separation of critical nuclei), the density profile of an infinite crystal gradually becomes more and more diffuse. (This is true even at equilibrium if the temperature is greater than T_R. See Sections V and VI.)

This effect can be seen most clearly in the limit where evaporation is completely neglected. It is easy then to solve exactly for the $C_n(t)$ and the $f_{n;m}(t)$ and show that, despite the constant growth rate in this limit, the $C_n(t)$ never rigorously obey the steady-state conditions (3.15).[16] However, the rate of change of the interface width is very small compared to the growth rate of the crystal. Thus (3.15) and (3.16), which relate conditions on adjacent layers, hold to a very good approximation even in this rather artificial limit. Nevertheless, the steady-state ($t \to \infty$) profile is infinitely diffuse.

Under more realistic conditions, evaporation considerably inhibits the increasing diffuseness of the profile. In fact, a finite crystal then develops a well-defined steady-state growth profile whose width should depend only very weakly on the size of its cross-sectional area once it is much greater than the size of a critical nucleus. By assuming steady-state conditions as in (3.15) and (3.16), we are implicitly considering the local profile and effective evaporation rate of such a finite system. In the practical case where one studies steady-state growth on a finite crystal, (3.15) and (3.16) should be exact.

Assuming (3.15) and (3.16) hold, we can define continuous functions of the variable $x \equiv n - \bar{R}t$ such that

$$C_n(t) \equiv c(n-\bar{R}t) \equiv c(x) \tag{3.17}$$

and

$$k(n,t) \equiv k(n-\bar{R}t) \equiv k(x) \tag{3.18}$$

Here, $\bar{R}$, the average growth rate, is given by

$$\bar{R} = 1/\tau \tag{3.19}$$

where τ is the time required to deposit a monolayer on the surface. Equation 3.6 can then be rewritten with the help of (3.17) and (3.18) as

$$-\bar{R}\frac{dc(x)}{dx} = k^+[c(x-1)-c(x)] - k(x)[c(x)-c(x+1)] \tag{3.20}$$

At high deposition rates or high temperatures, the local profile $c(x)$ is a slowly varying function of x. That is, for fixed time t, $C_n(t)$ changes only a small amount from $C_n(t)$ to $C_{n\pm1}(t)$ or, for fixed n, $C_n(t)$ is smoothly varying in time from t to $t \pm \tau$. Then a Taylor series expansion of $c(x \pm 1)$ about $c(x)$ should be a good approximation:

$$c(x \pm 1) = c(x) \pm \frac{dc(x)}{dx} + \frac{1}{2}\frac{d^2c(x)}{dx^2} \pm \ldots \tag{3.21}$$

We assume here that this expansion is valid under all conditions. We keep terms through second order in the expansion (3.21) and substitute them into (3.20); expansion at least through second order is necessary to distinguish between the derivative on the left-hand side of (3.20) and the finite differences on the right. This gives the differential equation

$$-\bar{R}\frac{dc(x)}{dx} = k^+\left[-\frac{dc(x)}{dx} + \frac{1}{2}\frac{d^2c(x)}{dx^2}\right] + k(x)\left[\frac{dc(x)}{dx} + \frac{1}{2}\frac{d^2c(x)}{dx^2}\right] \tag{3.22}$$

Defining

$$\rho(x) \equiv -dc(x)/dx \tag{3.23}$$

and integrating, we get

$$\rho(x)=\rho(0)\exp\left[\int_0^x \frac{2(k^+-k(y)-\bar{R})}{k^++k(y)}dy\right] \tag{3.24}$$

The origin of the coordinate system in x has not yet been fixed. We choose it such that

$$c(0)=\tfrac{1}{2} \tag{3.25}$$

Then, since $c(-\infty)=1$ and $c(\infty)=0$, we have

$$c(x)=1-\int_{-\infty}^{x}\rho(y)dy=\int_x^{\infty}\rho(y)\,dy \tag{3.26}$$

where $\rho(x)$ is given by (3.24), and (3.25) requires

$$\int_{-\infty}^{0}\rho(x)\,dx=\int_0^{\infty}\rho(x)\,dx \tag{3.27}$$

Equations 3.24 to 3.26 give the average growth rate $\bar{R}$ and profile $c(x)$ in the steady-state continuum approximation as a function of the effective evaporation rate $k(x)$. The latter of course is unknown. If we use the Temkin expression, (3.14), for $k(x)$, we obtain a complicated nonlinear integral equation. This choice is only an approximation, but it does express the basic physical fact that the effective evaporation rate is less when surface atoms have many neighbors (on the average) than when they have few.

We consider here an extremely simple approximation for $k(x)$ which still maintains this essential physical feature but also allows (3.24) to (3.26) to be solved analytically:

$$\begin{aligned} k(x)&=k_s; \quad x\leq 0 \\ &=k_f; \quad x>0 \end{aligned} \tag{3.28}$$

Here k_s and k_f are constants (which may depend on T, k^+, and the rate of surface migration) whose values will be chosen later. Using (3.25), (3.28) asserts that the effective evaporation rate is some "slow" constant value k_s for layers that are more than half-filled (these presumably have more nearest neighbors) and some "fast" constant value k_f for layers that are less than half-filled (these presumably have fewer nearest neighbors). Clearly $k_f>k_s$. We refer to this approach as the two rate model.

One possible (but rather extreme) choice for these parameters is

$$\begin{aligned} k_s &= \nu e^{-4\beta\phi} \\ k_f &= \nu \end{aligned} \tag{3.29}$$

Here we approximate the effective evaporation rate by that of isolated adatoms if the layer is less than half-filled and that of a completely filled layer if it is more than half-filled. More realistic choices are discussed later. We consider now the qualitative conclusions one can make independent of the particular choice of these parameters.

Substituting (3.28) into (3.24), we find

$$\rho(x)=\rho(0)\exp\left\{\frac{2(k^+-k_s-\bar{R})x}{k_s+k^+}\right\}, \quad x<0 \tag{3.30}$$

$$\rho(x)=\rho(0)\exp\left\{\frac{2(k^+-k_f-\bar{R})x}{k_f+k^+}\right\}, \quad x>0 \tag{3.31}$$

Equation 3.27 then implies

$$\frac{2(k^+-k_s-\bar{R})}{k_s+k^+}=\frac{-2(k^+-k_f-\bar{R})}{k_f+k^+} \tag{3.32}$$

thus determining the average growth rate $\bar{R}$ as

$$\bar{R}=\frac{(k^+)^2-(k_sk_f)}{k^++[(k_s+k_f)/2]} \tag{3.33}$$

Then the interface profile $c(x)$ from (3.25) and (3.26) is

$$\begin{aligned} c(x)&=\tfrac{1}{2}e^{-x/L}, \quad x>0 \\ &=1-\tfrac{1}{2}e^{x/L}, \quad x<0 \end{aligned} \tag{3.34}$$

where L is

$$L=\frac{k^++[(k_s+k_f)/2]}{k_f-k_s} \tag{3.35}$$

L gives a measure of the interface width.

Equation 3.33 shows that $\bar{R}=0$ when $k^+=(k_sk_f)^{1/2}$. Since there is no growth at equilibrium, we fix the product $(k_sk_f)^{1/2}$ as

$$(k_sk_f)^{1/2}=k_{eq}=\nu e^{-2\beta\phi} \tag{3.36}$$

Note that the choices for k_s and k_f in (3.29) obey (3.36). Having required (3.36) to hold, there is only one parameter, say,

$$\bar{k}\equiv(k_s+k_f)/2 \tag{3.37}$$

left free to vary.

Recalling the WF growth rate, (3.12), and using (3.37), the average growth rate in (3.33) can be written as

$$\bar{R}=\frac{(k^+)-k_{eq}^2}{\bar{k}+k^+}=R_{\mathrm{WF}}\left[\frac{k_{eq}+k^+}{\bar{k}+k^+}\right] \tag{3.38}$$

The interface width L in (3.35) can also be written, using (3.31) and

(3.37), as

$$L = \frac{\bar{k} + k^+}{\sqrt{\bar{k}^2 - k_{eq}^2}} \tag{3.39}$$

Equation 3.38 shows that the growth rate tends to the WF result for two limiting cases. The first is at very high deposition rates where $k^+ \gg \bar{k}$. The second is at very high temperatures where $\beta\phi \ll 1$. Then, $k_s \to k_f$, since the effects of the bonds on the evaporation rate become unimportant. From (3.36) to (3.38) we see $\bar{R} \to R_{WF}$.

Note that the interface width given by (3.39) becomes increasingly large as either the deposition rate or the temperature is increased, in agreement with MC calculations and physical intuition.

Since k_f must be positive, we can define a new parameter $\bar{c}$ such that

$$k_f = \nu e^{-4\beta\phi\bar{c}} \tag{3.40}$$

In analogy with the Temkin expression, (3.14), we physically interpret $\bar{c}$ as some "effective" probability per surface atom of finding a neighboring site occupied when averaged over the region $x > 0$. Using (3.36) and (3.37), we then have

$$\bar{k}/k_{eq} = \cosh[\alpha\beta\phi] \tag{3.41}$$

where

$$\alpha \equiv 2(1 - 2\bar{c}) \tag{3.42}$$

Using (2.3), (3.33), and (3.39), the growth rate can be written

$$\frac{\bar{R}}{k^+} = \frac{2\sinh(\beta\Delta\mu)}{\exp(\beta\Delta\mu) + \cosh(\alpha\beta\phi)} \tag{3.43}$$

and the interface width is

$$L = \frac{\exp(\beta\Delta\mu) + \cosh(\alpha\beta\phi)}{\sinh(\alpha\beta\phi)} \tag{3.44}$$

On physical grounds the parameter $\bar{k}$ and hence $\bar{c}$ or α should be a function of the temperature and the deposition and surface diffusion rates. Here we take a semiempirical approach and choose α to best fit experimental data. We rather arbitrarily choose α such that the growth rate given in (3.43) agrees with the MC value for $\beta\phi = 4$ when $\bar{R}/k^+ = \frac{1}{2}$. This choice is $\alpha = 1.3$ or $\bar{c} = 0.175$. Figure 4 compares the growth rates given by (3.43) with $\alpha = 1.3$ to the MC calculations for several different values of $\beta\phi$. Note that only the point at $\beta\phi = 4$ and $\bar{R}/k^+ = 0.5$ has been used to fit the parameter α. Figure 5 repeats the most physically relevant part of the data on an expanded scale. No surface diffusion was allowed in the MC results.

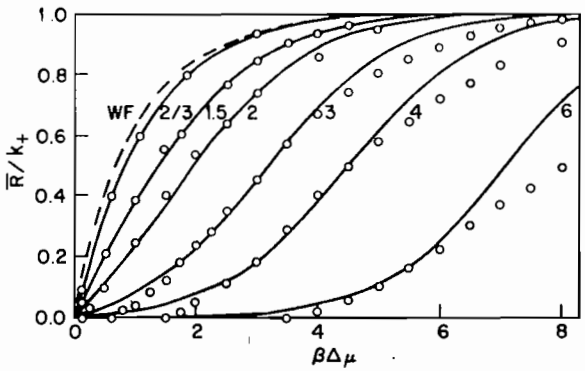

Fig. 4. The growth rate as calculated by the two-rate model, solid curves, is compared to MC data, circles, for a wide range of parameters. The number adjacent to the circles indicates the value of $\beta\phi$, and the dashed curve is the Wilson-Frenkel rate.

There is good qualitative agreement between theory and computer "experiment" over a very wide range of choices of temperature and deposition rate. In the region of high temperature and high deposition rates, where the original assumptions leading to the model are valid, the theory provides quantitatively accurate results.

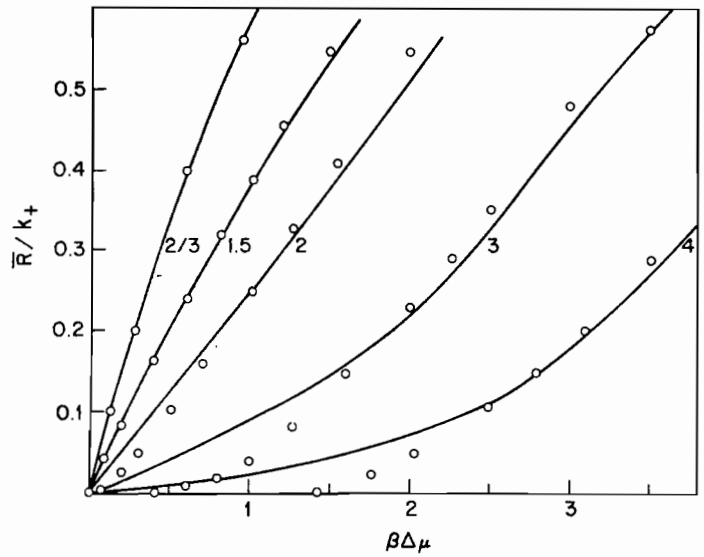

Fig. 5. An expanded plot of some of the data shown in Fig. 4.

The theory is least accurate in the region of low temperatures and low deposition rates, precisely that region in which the continuum approximation and our crude estimates for $k(x)$ are most in error. Figure 5 concentrates on this region. Equation 3.43 predicts that as $\beta\Delta\mu \to 0$ or $k^+ \to k_{eq}$

$$\bar{R}/k^+ \propto \beta\Delta\mu \tag{3.45}$$

In the low temperature, low deposition rate region, growth occurs by a nucleation mechanism, and the expected dependence is (see Section IV)

$$\bar{R}/k^+ \propto \exp(-c/\beta\Delta\mu) \tag{3.46}$$

For small $\beta\Delta\mu$, (3.43) predicts growth rates whose magnitudes are very large relative to those of (3.46).

However, the actual growth rate is in any case very small in this region, and (3.43) is not far off in absolute magnitude from the MC results. Furthermore, the theory gives the correct temperature dependence of the growth rate.

The above results were derived assuming that there was no surface diffusion. The qualitative effects of surface diffusion show up in the two rate model in the choice of the parameter $\bar{c}$. Because clustering is enhanced with surface diffusion present, a larger value of $\bar{c}$ or, equivalently, a smaller value of α would be appropriate. Using (3.43), we see that the growth rate of a crystal with surface diffusion (and smaller α) is equal to that of a system without surface diffusion but at a smaller value of $\beta\phi$. Within the two rate model, then, the effect of surface diffusion is to shift the growth rate curves in Fig. 4 toward the WF result. This conclusion is in qualitative agreement with MC simulations at temperatures above T_R or for high driving forces.

Thus in general the two rate model has proven very successful. We have made the simplest possible assumption about the effective evaporation rate $k(x)$ which still maintains the essential physical feature that atoms with many nearest neighbors evaporate more slowly than do atoms with few neighbors. This assumption allowed us to derive analytic expressions for the growth rate and interface profile in the continuum steady-state approximation. These expressions give a qualitatively correct description of the growth rate and density profile over a very wide range of deposition rates and temperatures. Above the roughening temperature, the theory is in quantitative agreement with the MC results.

Below T_R the predicted growth rate is very small for small driving forces. However, the theory fails to predict a qualitative change in the growth rate at the roughening transition. The relative accuracy of the theory at low temperatures arises from a fortuitous cancellation of errors between the continuum approximation and two rate approximation for $k(x)$, and not to a correct description of the fundamental physics in the nucleation regime. Furthermore, the subtleties of the roughening transition cannot be dealt with by such simple methods as these. The next sections discuss the more complicated theories needed in these cases.

IV. NUCLEATION THEORY OF CRYSTAL GROWTH

A. Classical Theory of Heterogeneous Nucleation

When the temperature is far below the roughening point, none of the approximations described above is very accurate at small values of the driving force. It is necessary to include the formation of large clusters of atoms that play an essential part in the 2d nucleation process. In fact, deposition on a low index face in this regime can be described in terms of the random nucleation of 2d clusters of atoms that expand and merge with one another to form complete layers. As we shall see, a good approximation for the crystal growth rate can be obtained if accurate values of the 2d nucleation rate are available.

We first employ the classical Becker-Doering theory[7] to calculate the 2d nucleation rates on the SC(001) face. This theory provides a basis for the development of a more detailed atomistic nucleation theory. Both theories are then compared directly with a MC simulation that is specifically designed to compute nucleation rates.

Suppose that a crystal surface initially in equilibrium with its vapor at low temperatures is subjected to a finite driving force. At first most of the clusters on the surface contain only a few atoms because of the small vapor pressure corresponding to the low temperature and driving force. The small clusters are more likely to lose atoms by evaporation than to expand, since the atoms at their periphery are only weakly bonded to the crystal. However, there may be a few clusters present that are large and compact. These are more likely to grow to larger sizes. These "supercritical" clusters can be generated only by an improbable series of impingement and evaporation events, but once they are formed, they usually grow until they cover the entire crystal face or merge with other clusters at the same level.

We derive the rate of nucleation of supercritical clusters in terms of the net rates of promotion of clusters along the sequence of increasing sizes until they become stable against decomposition. At the beginning of the sequence, the net rate at which empty sites are promoted to single adatoms is

$$I_0 = k^+ - n_1\nu \tag{4.1}$$

where n_1 is the average number of adatoms per site. Note that k^+ is an accurate expression for the rate of creation of adatoms when only a small number of the surface sites are located adjacent to adatoms or clusters. Again, this is valid for small values of the driving force. (In general k^+ represents an upper bound to this rate.)

Generalizing this procedure, we define the net rate of promotion of the n_i clusters containing i atoms to size $i+1$ as

$$I_i = \gamma_i^+ n_i - \gamma_{i+1}^- n_{i+1} \tag{4.2}$$

where γ_i^+ is the average rate of attachment of atoms to a cluster containing i atoms, and γ_{i+1}^- is the average rate of detachment from a cluster of $i+1$ atoms. We neglect the merger of two or more clusters in these equations, since the density of clusters is small.

The crux of nucleation theory is the evaluation of γ_i^+ and γ_{i+1}^-. A cluster of i atoms may exhibit a large number of different configurations, since the only requirement is that each atom be joined to another atom in the cluster by nearest-neighbor bonds. Thus the γ's are averaged over clusters with a large variation in condensation and evaporation rates. Furthermore, the densities of the various cluster configurations depend on both the temperature and the driving force. Several procedures have been proposed to solve this problem. One method that is accurate at very low temperature and high driving force is to include only the lowest energy configurations in the computation.[19,20] Exact values for the γ's can then be calculated, but the nucleation rates obtained always represent a lower limit to the actual rate.

The classical theory[7] makes use of an artificially constrained equilibrium to evaluate γ^+ and γ^-. We imagine that a constraint is imposed on the system that prevents clusters above a certain finite size from growing. The system then reaches a new (constrained) equilibrium state where the steady-state nucleation rate is zero, even in the presence of a large driving force. The cluster concentrations take on values $n_i^{(o)}$ corresponding to a state in which the net rates of creation and annihilation of all cluster sizes are equal. Thus, according to (4.2),

$$\gamma_i^+ n_i^{(o)} = \gamma_{i+1}^- n_{i+1}^{(o)} \tag{4.3}$$

This equation also follows directly from the principle of microscopic reversibility. Equation 4.3 is then used to eliminate γ_{i+1}^- in (4.2), and the result is

$$I_i = \gamma_i^+ n_i^{(o)} \left[\frac{n_i}{n_i^{(o)}} - \frac{n_{i+1}}{n_{i+1}^{(o)}} \right] \tag{4.4}$$

This expression is particularly useful for the evaluation of the nucleation rate under steady-state conditions, where $I_i = I$ for all i. Then (4.4)

can be solved for I, provided n_j for some particular j is known or can be approximated. Very accurate expressions for the nucleation rate are obtained if we set $n_j = 0$, where j is sufficiently large that the corresponding cluster is not likely to decompose. The larger clusters usually merge with one another and are, in a sense, removed from the system in the form of new layers of the crystal. Dividing both sides of (4.4) by $\gamma_i^+ n_i^{(o)}$ and then summing over i, we obtain

$$I \sum_{i=0}^{j-1} \frac{1}{\gamma_i^+ n_i^{(o)}} = \frac{n_0}{n_0^{(o)}} \cong 1 \tag{4.5}$$

where $n_j = 0$ is assumed. Note that n_0 and $n_0^{(o)}$ are the fractions of empty sites during nucleation and at equilibrium, and both are approximately unity under the assumed conditions.

The values of γ_i^+ and $n_i^{(o)}$ in (4.5) can be experimentally estimated from the macroscopic diffusion rates and surface free energies in the case of 3d nucleation.[21] However, the properties of small surface clusters are very different from those in bulk material; furthermore, in the case of 2d nucleation, the macroscopic properties are not usually available. Therefore we derive expressions for $n_i^{(o)}$ on the SC(001) face from a theoretical estimate of the excess free energy associated with the presence of a cluster of i atoms,

$$\Delta G_i \cong (\phi/2) \cdot 4\sqrt{i} - i\Delta\mu \tag{4.6}$$

Here $\phi/2$ is the energy of a broken bond, and the number of broken bonds at the edge of a cluster is approximated by $4\sqrt{i}$, the exact value for square clusters. The last term in (4.6) represents the free energy gained in the transfer of atoms from the fluid to the crystal. If nucleation involves large clusters at high temperatures, the configurational entropy of the cluster should also be included in (4.6). This can be done by replacing the $T=0$ edge energy $\phi/2$ by the step edge free energy (see Ref. 22 for a theory of the equilibrium properties of steps at finite temperatures). This is useful in cases in which the critical clusters are very large and the edge free energy per unit length is approximately equal to that of an infinite step. For the present calculation at low temperatures, the edge energy differs negligibly from the edge free energy, and the simple expression in (4.6) can be used. Accordingly,

$$n_i^{(o)} \cong \exp\left[\beta i\Delta\mu - 2\beta\phi\sqrt{i}\right] \tag{4.7}$$

The exponential has its minimum value when $i = i^* \cong (\phi/\Delta\mu)^2$, and this defines the *critical cluster size*. Clusters with $i \gg i^*$ have large equilibrium concentrations, since the free energy $i\Delta\mu$ gained by the transfer of atoms from the fluid to the crystal is much greater than the edge energy, $2\phi\sqrt{i}$.

The nucleation rate is derived from (4.5) and (4.7),

$$\frac{I}{k^+} \cong \left[\tfrac{1}{4}\sum_{i=0}^{i-1} \exp\left[-\beta i \Delta\mu + 2\beta\phi\sqrt{i}\right] i^{-1/2}\right]^{-1} \tag{4.8}$$

where the approximate expression $\gamma_i^+ = 4k^+\sqrt{i}$ is used. This value for γ^+ is exact in the case of direct impingement on the sites at the peripheries of square clusters. Here we have excluded surface diffusion. However, adatoms may also contribute to γ_i^+ when their mobility is large. Later we consider some of the effects of surface diffusion on the nucleation process. It is apparent that mobile adatoms may cause a dramatic increase in γ^+ and hence in I. Note that the sum in (4.8) is dominated by the terms in the vicinity of i^*, and the result is not at all sensitive to the value chosen for j provided that $j \gg i^*$.

An analytical expression for I is obtained if we replace the sum in (4.8) by an integral and change variables to $y = \sqrt{i}$:

$$\frac{I}{k^+} \cong \left[\tfrac{1}{2}\int_0^\infty e^{-\beta\Delta\mu y^2 + 2\beta\phi y}\, dy\right]^{-1}$$

or

$$\frac{I}{k^+} \cong \left[\tfrac{1}{2}\exp\left[\beta\phi^2/\Delta\mu\right](\beta\Delta\mu)^{-1/2}\int_{-\phi\sqrt{\beta/\Delta\mu}}^{\infty} e^{-\xi^2}\, d\xi\right]^{-1} \tag{4.9}$$

If $\Delta\mu \ll \beta\phi^2$, we have the simple result

$$I/k^+ = \frac{\sqrt{\pi\beta\Delta\mu}}{2}\exp\left[-\beta\phi^2/\Delta\mu\right] \tag{4.10}$$

and even when $\Delta\mu \to \infty$ this expression is half that of (4.9).

The nucleation rate in (4.10) is the result of a number of approximations, and for this reason it is important to test its validity before deriving expressions for the crystal growth rate. Furthermore, a test of this result also provides information on the validity of the classical approach to nucleation. Several authors have measured heterogeneous nucleation rates by the MC method.[23,24] Here we report some of our recent MC data and an atomistic nucleation theory that corresponds precisely to the conditions of the simulation model.[25] By utilizing the control over the atomic processes afforded by the MC method, we measured the nucleation rates directly without the complicating effects caused by the merger of large clusters.

We simulate nucleation on the SC(001) face using exactly the same transition probabilities employed for the growth rate calculations mentioned earlier. However, in this case a current list is maintained that contains all clusters of two or more atoms, together with the locations of

the atoms that are a part of each cluster. Whenever the number of atoms in a cluster exceeds twice the number in the critical cluster, it is removed from the surface. That is, the heights of the columns corresponding to atoms in that large cluster are each reduced by one atomic spacing. In this way, only the clusters that have an important part in nucleation are present at any time. The nucleation rate is proportional to the rate at which clusters are removed. As one would expect, the rate of removal was essentially unchanged in one simulation in which the clusters were allowed to grow to a larger size.

The MC nucleation data are plotted as symbols in Fig. 6 as a function

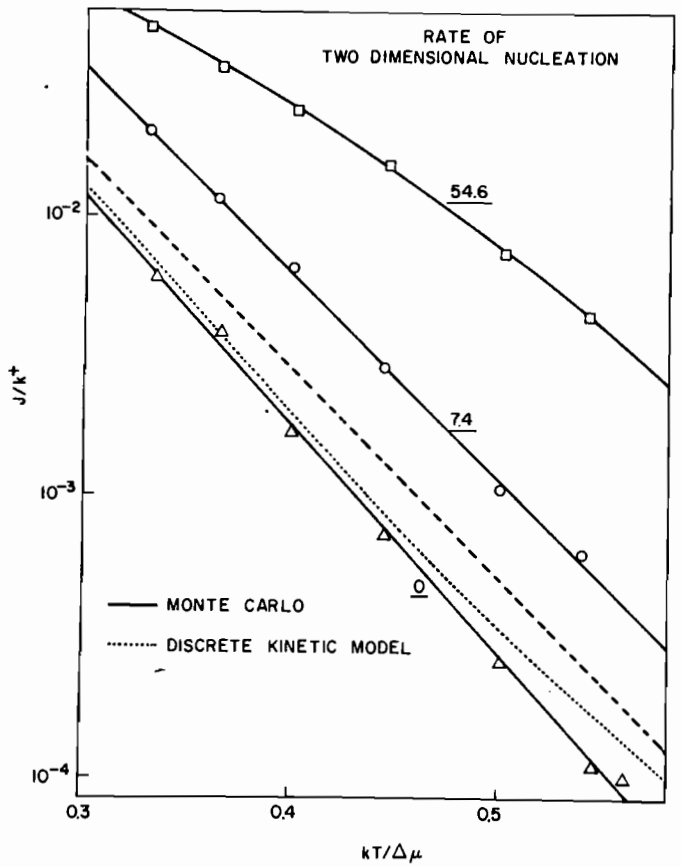

Fig. 6. Comparison of MC data on 2d nucleation rates with theory. The symbols with the solid curves through them are MC data. The numbers adjacent to these curves are the ratio of the migration to evaporation rates. The dashed curve is the classical nucleation rate (4.10). The dotted curve is the nucleation rate predicted by the atomistic nucleation theory.

of $1/\beta\Delta\mu$. Several values of the surface mobility are included, but the curve labeled with 0 corresponds to immobile adatoms as was assumed in the theory discussed here. The temperature $kT/\phi = 0.25$ is less than half of the roughening temperature, and entropy effects should be small, since the edge free energy of a step is only slightly less than the edge energy. The nucleation rate predicted by (4.10) is indicated by the dashed curve; this result is somewhat higher than the MC data corresponding to zero mobility. In view of the approximate (upper bound) value of γ^+ employed in the derivation of (4.10), this discrepancy is not surprising. The expression in (4.10) is nearly linear in this plot. The fact that the MC data are approximately linear with the same slope is a good indication that the classical theory contains the essential physics in this case.

The primary effect of mobile adatoms is to increase the rate at which atoms arrive at empty sites on the surface. In addition to impinging directly from the vapor, atoms already on the surface may jump to neighboring vacant sites. If the surface were in equilibrium with the vapor, the argument of microscopic reversibility implies that the rate of impingement on an empty site would be increased by the factor $1+K_m/K^-$, where K_m/K^- is the ratio of the frequencies of migration to evaporation. The MC data labeled 7.4 corresponds to $K_m/K^- = 7.4$, and indeed at small $\Delta\mu$ values they are approximately 8.4 larger than the zero mobility data. At the larger $\Delta\mu$ values, kinetic effects are apparently important, and a smaller increase is observed. The data with $K_m/K^- = 54.6$ exhibits a correspondingly large nucleation rate only at the smallest values of $\Delta\mu$. At large $\Delta\mu$ values, a much smaller increase is measured. When $\Delta\mu = 3kT$, about 30% of the atoms that impinge on the surface are removed with the supercritical clusters. This rapid removal rate depletes the adatom population far below the value corresponding to equilibrium, and hence the microscopic reversibility argument is not appropriate.

B. Atomistic Nucleation Theory

A qualitatively different approach to nucleation is possible when the critical nucleus is very small, as is usually the case in most vapor deposition and molecular beam experiments. Then it is feasible to solve numerically, without approximation, detailed kinetic equations that determine the concentrations of all of the clusters near the critial size. The time dependence of the adatom concentration is governed by the equation

$$\frac{dn_1}{dt} = k^+ + 2k_1^- n_2 - (4k^+ + k_0^-)n_1 \tag{4.11}$$

The first two terms on the right-hand side account for the formation of adatoms by direct impingement and by the disintegration of dimers, respectively. The other terms represent the depletion of the adatom population by a direct impingement on one of the four neighboring sites to produce a dimer (surface migration is excluded), and by evaporation. Similarly, the rate of change of the dimer population is

$$\frac{dn_2}{dt} = 4k^+ n_1 + 2k_1^- n_3 - (6k^+ + 2k_1^-)n_2 \tag{4.12}$$

The number and complexity of the equations increases when larger clusters are considered. In the case of the three-atom clusters, it is necessary to distinguish between the different possible configurations, as illustrated in Fig. 7.

We have programmed the equations for all possible configurations of clusters containing less than seven atoms. We count as the nucleation rate the rate of formation of seven-atom clusters, and these are not allowed to disintegrate. The equations are integrated with respect to time by the Runge Kutta method starting at $t = 0$ with $n_i(0) = 0$. When the $n_i(t)$ reach stationary values corresponding to the steady state, the nucleation rate is determined.

The results of this calculation are indicated in Fig. 6 by the dotted curve. This curve is within the statistical error of the MC data at all points except for the smallest values of $\Delta\mu$. Here the critical cluster size is in the vicinity of seven atoms, and it is not valid to assume that none of the seven atom clusters will disintegrate. This is probably the best agreement

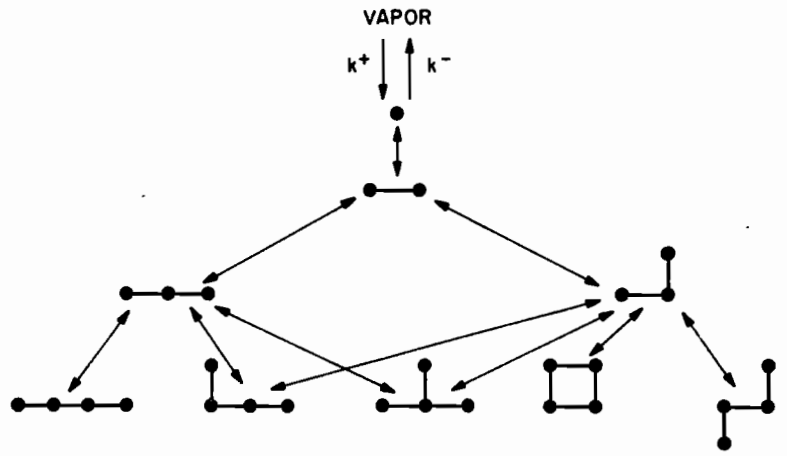

Fig. 7. Schematic diagram of the cluster "reactions" involved in nucleation on a SC(001) face. All configurations of clusters with four or less atoms are included.

between a nucleation theory and "experiment" that has been obtained. Although the theory is designed specifically to correspond to this particular MC model, the excellent agreement justifies two basic assumptions of nucleation theories in general: (*a*) the predominance of single atom additions and removals in the kinetics of cluster growth and decay and (*b*) the dominant effect of clusters close to the critical nucleus in size in determining the nucleation rate.

C. Interface Motion by 2d Nucleation

The crystal growth rate is completely determined by the nucleation rate I in certain limiting cases. If the time between nucleation events is very large, then each such event results in the growth of a complete layer of atoms,[26] and

$$R = aIN_0 \qquad (IN_0 \ll v/L) \tag{4.13}$$

Here a is the layer spacing; N_0 is the number of sites on the close-packed face, v is the average speed of expansion of the edge of a cluster, and L is the largest linear dimension of the face. The condition on I requires that the average time between nucleation events should be much longer than the time necessary for a cluster to expand and cover the entire face. Hence it is unlikely that two or more clusters would contribute to the growth of the same layer. In this limiting case, the growth rate is proportional to the surface area through the term N_0. In practice, this relation is normally applicable only to the kinetics of minute crystals or to growth rates that are so small that they are difficult to measure. Electrocrystallization provides a notable exception, since the rate of growth is proportional to the current to the electrodes and very small currents can be detected. Budevski et al.[27] applied voltage pulses to generate isolated clusters on silver crystals in small capillaries. They were then able to monitor the rate of expansion of the cluster by measuring the subsequent current flow at a potential that was too small to induce appreciable nucleation.

In most cases of practical importance, a very large number of clusters nucleate at each level, and the growth rate is independent of the surface area, but instead is determined by the rate at which the clusters nucleate and merge with one another. Kolmogoroff was the first to obtain an exact analysis of a restricted version of this problem.[28] His result is limited to the first layer deposited onto an initially flat substrate, but it also provides an estimate of the multilevel growth rate and illustrates most of the essential features of this problem.

Kolmogoroff's analysis can be applied to the nucleation of circular clusters that expand with a constant radial velocity v. Also, we assume a

constant nucleation rate I starting at $t = 0$. (The nucleation induction time is assumed to be negligible in comparison with the time required to deposit a layer.) Then we can calculate the probability $x_1(t)$ that an arbitrary point in the first layer is covered by a cluster. First consider the probability q_i that a nucleus formed during the interval $(t_i, t_i + \Delta t_i)$ would cover the point before time t ($t_i < t$). The density of clusters nucleated during Δt_i is $\rho I \Delta t_i$, where ρ is the number of sites per unit area of the surface. Only those nucleated within a radius $v(t - t_i)$ of the point will reach it before time t, and hence

$$q_i = \pi v^2 (t - t_i)^2 \rho I \Delta t_i \tag{4.14}$$

The probability that the point remains uncovered at time t is the product of the probabilities that it did not get covered by nucleation events during all of the subintervals Δt_i in t, that is,

$$1 - x_1(t) = \prod_i (1 - q_i) \tag{4.15}$$

We may use the relation $1 - q_i \cong \exp(-q_i)$ in (4.15) and (4.14) to derive the exact result (in the limit as $\Delta t_i \to 0$)

$$1 - x_1(t) = \exp\left[-\pi I \rho v^2 \int_0^t (t - t')^2 \, dt'\right] \tag{4.16}$$

Performing the integration using the dimensionless time variable $\tau = t(I\rho v^2)^{1/3}$, we have

$$x_1(\tau) = 1 - \exp\left[-\frac{\pi}{3}\tau^3\right] \tag{4.17}$$

Several authors have treated the multilevel deposition process by analytical techniques[26,29–32] and by simulation.[33,34] None of the analytical methods is exact, but one of the more satisfactory approaches is to employ the exact rate of deposition on the first layer

$$r_1(\tau) \equiv \frac{dx_1}{dt} = (I\rho v^2) \exp\left(-\frac{\pi}{3}\tau^3\right) \tag{4.18}$$

to derive an approximation for the asymptotic growth rate R as $t \to \infty$. During the interval $(t', t' + \Delta t)$ a fraction of the nth layer $r_n \Delta t$ is deposited. We then assume that the rate of deposition on this segment of layer n at a later time is equal to that on the substrate after the same elapsed time. Then (4.18) can be used to relate $r_{n+1}(t)$ to $r_n(t)$, that is,

$$r_{n+1}(t) = \int_0^t r_n(t') r_1(t - t') \, dt' \tag{4.19}$$

Actually, the deposition on the various segments of layer n is not exactly equivalent to deposition on the substrate. At $t=0$, the substrate layer is complete, and no clusters are present at the next level. However, at any finite t', both layer n and layer $n+1$ are partially filled. An incomplete layer n should reduce the deposition rate in comparison with that on the substrate at the corresponding time, but the clusters already deposited at level $n+1$ will have the opposite effect. Because of these opposing influences, the total deposition rate on all levels predicted by (4.19) may be rather accurate. Then we assume that the instantaneous growth rate R_i is

$$R_i(t)=\sum_{n=1}^{\infty} r_n(t) \tag{4.20}$$

where the $r_n(t)$ are obtained from (4.19).

The $r_n(t)$ are most easily evaluated in terms of Laplace transforms, since (4.19) is expressed as a convolution of r_n and r_1. In the limit of $t\to\infty$, the steady-state deposition rate is obtained directly from the Laplace transformations, and the result is (see Ref. 30)

$$R=(I\rho v^2\pi/3)^{1/3}/\Gamma(4/3)=1.137(I\rho v^2)^{1/3} \tag{4.21}$$

We emphasize that this is not an exact solution to the multilevel deposition rate, although it has been represented as such. It is perhaps worthwhile to compare this with other estimates. The maximum rate of deposition r_1 in the first layer has been suggested as an approximation for R, and from (4.18) we obtain the value $r_1^{\max}\cong 1.194(I\rho v^2)^{1/3}$. In addition, Nielsen calculated the steady-state deposition rate by assuming a simplified surface structure.[26] His analysis yields the result $R\cong 1.015(I\rho v^2)^{1/3}$. Thus, although (4.21) is only an approximation to the asymptotic multilevel rate, it is apparently quite close to the exact value.

The edge velocity v depends on a number of factors, including the edge orientation, cluster size, and the temperature. Very small clusters have reduced edge velocities resulting from the small number of bonds connecting the atoms at the edge to others in the cluster. Once the cluster is about twice the critical size, however, this effect is small, and the edge velocity may be approximated by that of an infinite step. For our purposes it is sufficient to assume that $v\propto\Delta\mu$. This relation is always valid for small $\Delta\mu$, since the edge of a step is rough at all temperatures and there is a linear response to a small driving force. Large variations in the crystal growth rate due to changes in the temperature and driving force arise primarily from corresponding variations in I, and for this reason we have examined the nucleation process in some detail.

Crystal growth rates calculated by the MC method were discussed previously with reference to the two rate model. At low temperatures, the MC rates were significantly below the predictions of the two rate model, but it is precisely in this region that the nucleation theory described above is most appropriate. Using I from (4.10) and the relation $v\propto\Delta\mu$, (4.21) becomes

$$R\propto(\beta\Delta\mu)^{5/6}\exp[-\beta\phi^2/3\Delta\mu] \tag{4.22}$$

If a driving force $\Delta\mu$ is applied at $t=0$, the instantaneous growth rate $R_i(t)$ approaches an asymptotic value after an initial transient. Figure 8 is a plot of the average MC growth rates measured on 90 different 60×60 sections of SC (001) faces. Each section, initially in equilibrium with the vapor, was subjected to a sudden application of the driving force. The open triangles represent the growth rates simulated without surface migration; the open squares represent growth rates obtained in the presence of surface migration, where the migration rate to sites of equal coordination is 7.4 times the evaporation rate.

The growth rates exhibit damped oscillations around the asymptotic rate R represented by the dashed lines. The numbers above the curves indicate the total number of monolayers deposited. The minima correspond roughly to the points where a layer is complete, and only small clusters have been nucleated at the next level. The amplitude of the oscillations provides a measure of the correlation in the surface heights at different sites in the array. At the beginning, the majority of the sites are

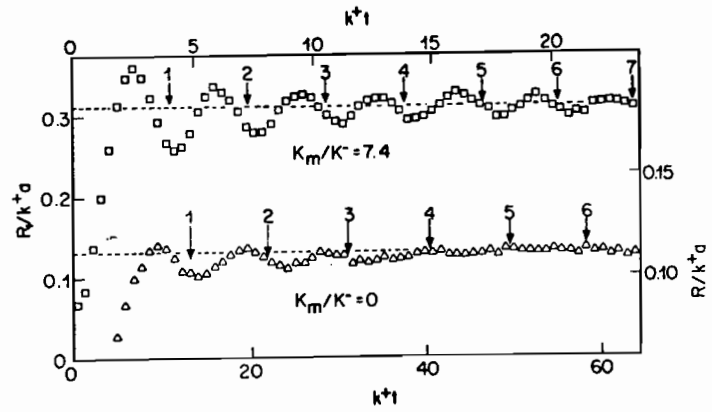

Fig. 8. The transient growth rates normalized by the impingement rate multiplied by the layer spacing. The squares represent data calculated with mobile surface atoms, and the figures at the left and above apply to this case. The triangles represent growth with immobile atoms, and the figures on the right and below apply here. Note that the growth rate scale does not extend to zero in this case. Here $\beta\phi=4$, $\beta\Delta\mu=2.5$. $\square\ k_m/k^-=7.4$ $\triangle\ k_m/k^-=0$.

at the same level, but later they are distributed over a range of levels as a result of statistical variations in the nucleation rates at the various locations. Sites close together remain highly correlated in height, since a cluster that nucleates near one site quickly spreads to the other. However, sites that are widely separated in the lateral dimension may eventually have large differences in height (see the discussion in Section III). In this case there should be little variation in the growth rate, since the different portions of the surface are experiencing the fast and slow growth regimes at different times. When the transient decays and the growth rate approaches R, the mean squared height deviations between such sites should be large and probably exceed one layer spacing.

Note the larger amplitude and greater persistence of the oscillations in the presence of mobile surface atoms. This is a consequence of the increase in the capture region near the cluster edges. Atoms that impinge within a distance of about three atomic diameters of the edge of a cluster have a good chance of migrating to the edge and being captured. This depletes the adatom concentration in this region. The surface heights of different sites remain correlated even after several layers have been deposited, since nucleation is suppressed on top of the smaller clusters. Many of the atoms that impinge on top of a cluster migrate to the edge and are captured at the lower level. The nucleation of clusters in the second layer, for example, generally occurs at a much higher coverage than was observed without surface migration.

The growth rates in Fig. 8 approach the asymptotic values quite rapidly. For example, the average growth rate during the deposition of the third monolayer is $\sim 0.97R$ without migration and $\sim 0.99R$ with migration. The maxima located at a time corresponding to about seven-tenths of a monolayer are greater than the asymptotic rate. This is in agreement with measurements of electrochemical deposition of silver on highly perfected silver crystals.[35] The more gradual increase derived from previous models[31,33,34] is probably a consequence of the idealized cluster shapes that were assumed. The clusters that appear during the MC simulation have a much longer periphery than the squares or circles assumed in the earlier models. As a result, a uniform coverage of the surface with cluster edges may occur with fewer clusters and a shorter transient results.

MC calculations for the asymptotic rates are compared with (4.22) in Fig. 9. The data indicated by triangles were measured in the absence of surface mobility; the dashed curve corresponds to (4.22) with $\beta\phi = 4$, the value employed in the simulation. The theory overestimates the growth rate at the larger values of $\Delta\mu$, because a significant fraction of the sites are adjacent to adatoms and clusters, and hence the assumptions used to

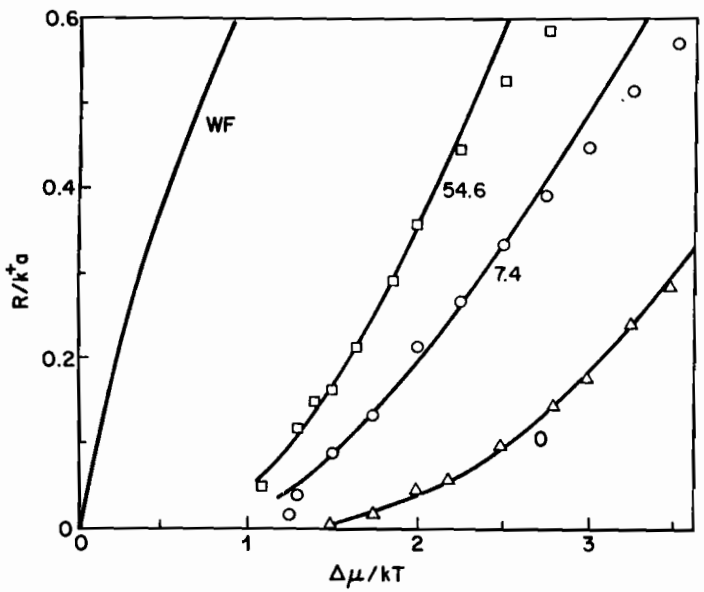

Fig. 9. MC calculations of the growth rates normalized by the impingement flux are indicated by the symbols for three values of the surface migration to evaporation ratio. The curves are derived from (4.22) except for the one labeled *WF*, which is a plot of (3.12). Again $\beta\phi = 4$.

derive the nucleation theory are not accurate. The solid curve through these data points was derived from (4.22), but with $\beta\phi = 4.4$. Thus a naive comparison of measured kinetic data with the 2d nucleation theory would suggest edge energies of clusters that are somewhat higher than the actual values.

Surface mobility causes large increases in the growth rates, and some important changes occur in the form of the growth rate curve. The adatom depletion zone around supercritical clusters can extend over large distances when they are highly mobile. Within this zone the nucleation rate is inhibited, and even a large cluster will expand more slowly if part of its periphery falls within the depletion zone of another cluster. At small values of $\Delta\mu$ the clusters are widely separated, and these effects are not important. In this region surface mobility induces the largest relative increase in the growth rate. At higher driving forces, where a dense array of clusters is nucleated, an appreciable fraction of the crystal surface may fall within the depletion zones. Then an increase in surface mobility causes a much smaller percentage change in R, and in fact, R approaches the maximum Wilson-Frenkel growth rate.

The MC growth rates with mobile adatoms are also compared with (4.22) in Fig. 9. The good agreement is somewhat surprising, since the derivation of (4.22) did not account for surface mobility. The curves were calculated with $\beta\phi = 3.2$ and 3.0 for surface mobility ratios $K_m/K^- = 7.4$ and 54.6, respectively. Thus in these cases the apparent edge energy of steps is *lower* than the actual value. This effect complicates the interpretation of experimental kinetic data.

We can conclude from the discussion of this section that growth rates of perfect crystals at low temperatures are determined primarily by the rate of 2d nucleation of clusters. The classical theory describes this process quite satisfactorily in the more idealized situations, for example when the surface mobility is low and the cluster density is low. In general, however, accurate calculations of edge free energies from kinetic measurements would require detailed information pertaining to the surface mobility. Later we discuss the 2d nucleation process in the presence of impurities, and here again we observe rather large changes in the kinetics. Crystal growth kinetics at low temperatures are extremely sensitive to the conditions in the interfacial region, and reliable interpretation of experimental data is possible only in the case of well-characterized systems.

V. THE SURFACE AT EQUILIBRIUM AND THE ROUGHENING TRANSITION

In the previous sections we discussed several different approaches to the dynamics of crystal growth. However, none of the theories was able to adequately describe the transition region between the nucleated growth regime below T_R and the continuous growth regime above T_R, or indeed even show the existence of the roughening transition. In this and the next section we examine this important transition region in some detail. We first consider the static (equilibrium) properties of a close-packed [SC (001)] face of an impurity-free perfect crystal.

At low temperatures, the interface is microscopically flat, with almost all columns the same height and only a few adatoms and surface vacancies present. As the temperature is increased, more energetic fluctuations allow for an increasing "roughening" of the surface as more and more columns slide up and down. The following argument, due in essence to Burton, Cabrera, and Frank[8], suggests that there should be a qualitative difference in the low and high temperature behavior of the interface because of a roughening phase transition.

We make use of the analogy between the lattice gas and a ferromagnetic Ising model, where an occupied site is represented by an "up" spin and a vacant site by a "down" spin.[36] Then the configuration at $T = 0$ is described in terms of 2d layers of up spins representing occupied sites in the crystal followed by layers of down spins representing the vapor. Consider the final (surface) layer of up spins. The layers directly above and below are magnetized in opposing directions, and their effects on the surface layer cancel; we have effectively an isolated 2d layer. This suggests that the crystal surface might behave like a 2d Ising model with large spin fluctuations (i.e., large regions of surface vacancies and adatoms) and thermodynamic singularities near the 2d critical temperature $kT/\phi = 0.57$.

This argument is merely suggestive, since there can be an exact cancellation only at $T = 0$. Indeed, using this idea, van Beijeren[37] has proven that the 2d critical temperature is a lower bound to T_R. Furthermore, the effects of surface roughening must extend over many layers. Nevertheless, using this one layer model, Burton, Cabrera, and Frank[8] and Jackson[3,38,39] had discussed many of the qualitative implications of surface roughening on crystal growth kinetics and morphology. The recent work reviewed below confirms their general picture and gives new insight into the true nature of the roughening transition.

The most graphic evidence for the effects of surface roughening comes from MC simulations of the SOS model.[9] Figure 10 gives typical equilibrium surface configurations generated by the MC method at various values of kT/ϕ. There seems to be a qualitative change in the surface somewhere between $kT/\phi = 0.57$ and $kT/\phi = 0.67$. At the lower temperature, distinct adatom and vacancy clusters are visible, but at the higher temperature the clusters have grown and merged together to such a degree that the original reference level of the surface is not apparent. It is already clear that crystal growth should be sensitive to the equilibrium structure. On a low temperature surface, the growth of a layer is a difficult process, requiring the formation of a large critical nucleus cluster. On a high temperature surface clusters of arbitrarily large size are already present at equilibrium, so the nucleation barrier disappears and continuous growth is possible. Further discussion of this point is given in Section VI.

Examination of these MC pictures suggests that there are several equivalent ways of characterizing the roughening transition. The size of an "average cluster" should diverge at the roughening temperature T_R. The formation of these arbitrarily large ridges also implies that the edge free energy and edge energy (per unit length) required to form a step on the crystal surface should vanish at T_R.[13] Since large clusters of adatoms and vacancies are equally probable at T_R, the average density of the surface layer should be $\frac{1}{2}$ at and above the roughening temperature. The formation of arbitrarily large clusters in one layer implies a high probability of finding similar large clusters in adjacent layers and the loss of the original reference level. Thus the interface width should diverge at T_R in

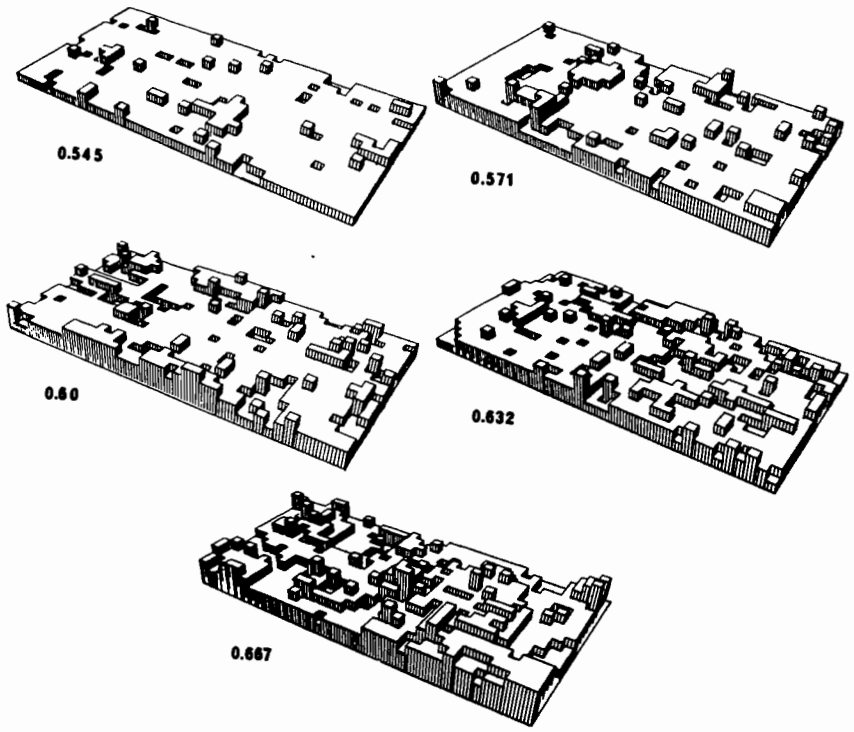

Fig. 10. Computer drawings of typical surfaces generated by the MC method at the indicated values of kT/ϕ.

an infinite system.[40] The disappearance of the nucleation barrier implies that the susceptibility (the partial derivative of the average height with respect to an infinitesimal driving force) should diverge at and above T_R.[41] The motion of the interface at and above T_R can be thought of as similar to that of a drumhead, whose normal modes of vibration correspond to the formation of large clusters of adatoms or vacancies on the surface.

The first theoretical evidence for this picture of the roughening transition using a multilayer model came from the series expansions of Weeks, Gilmer, and Leamy.[40,41] Low temperature series expansions for various measurements of the interface width and the susceptibility of the SOS model and the unrestricted lattice gas were calculated. The first nine terms of the series were evaluated, and over 3000 configurations contributed to the last term. The temperature at which each might diverge was estimated using standard series extrapolation methods which had been

successfully applied to study the critical point.[42] The method indeed indicated divergences at a roughening temperature slightly greater than the 2d Ising critical temperature, in agreement with the physical picture discussed above. Of course, these results are not conclusive because of the inherent uncertainties in series extrapolation methods. The different quantities appeared to diverge at slightly different temperature values (differing by less than 10%), so more terms in the series are clearly needed to obtain a completely consistent picture. However, the qualitative agreement obtained from the relatively short series calculated thus far seems most encouraging.

The MC simulations can also be used to estimate T_R.[43] In Fig. 11, we plot the difference in concentration between the surface layer and the layer directly above. As indicated above, this should vanish at T_R, and the data appear to confirm this expectation. Also plotted is the inverse of the fluctuation in particle number (related to the inverse susceptibility) which also appears to vanish at a temperature kT_R/ϕ slightly greater than 0.6. A recent estimate, 0.62 ± 0.01, was obtained using extensive MC data for the surface height correlations.[9B]

Swendsen has also used the MC method to estimate T_R for the SOS model.[14] His estimates for its value were based primarily on an apparent divergence in the specific heat and the step specific heat with system size at a particular T_R. However, the largest system size he used was 40×40, and our experience has been that this is the minimum size needed to obtain

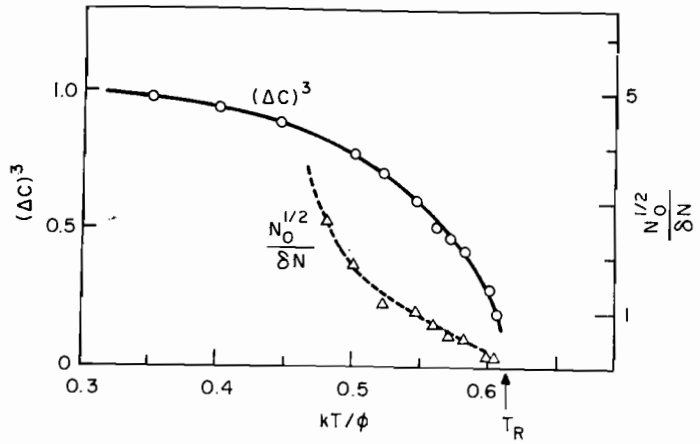

Fig. 11. MC data related to the difference in concentration ΔC in the layers bounding the $z = 0$ plane, and the reciprocal of the standard deviation δN of the number of atoms in the crystal.

accurate simulations near T_R. Thus his extrapolations using smaller system sizes are of questionable value. Furthermore, the best theoretical evidence (see below) indicates that there is no divergence in either of these quantities, but rather a maximum about 10% *below* T_R. Thus we believe that his estimate of $kT_R/\phi = 0.575 \pm 0.025$ is too low and is based on an incorrect assumption about the behavior of the specific heats.

The most definitive theoretical evidence for roughening comes from equivalence relations between models for the roughening transition and other models with a phase transition whose properties are already known. Chui and Weeks[10] considered the discrete Gaussian (DG) model of the interface with an interaction energy

$$E_{DG}(\{h_i\}) = -\frac{J}{2}\sum_{i,\delta}(h_i - h_{i+\delta})^2 \tag{5.1}$$

This differs from the ordinary SOS energy, (2.6), only in the energy assigned to neighboring columns differing in height by two or more units. The MC pictures show that such multiple height jumps between nearest neighbors are rare in the SOS model at the relatively low temperatures around the roughening point. Thus we expect (5.1) to give the same roughening behavior as does the ordinary SOS model, (2.6). (More generally, the roughening transition involves long wavelength fluctuations in the position of different parts of the interface. Changes in the interaction energy between columns that affect only the short wavelength properties should then be irrelevant at the roughening point.) Further, since the DG model assigns a greater energy to the multiple excitations, it is clear that roughening is more difficult than in the ordinary SOS model. If we can establish that the DG model has a roughening transition, then certainly the SOS model does.

Chui and Weeks showed that there is an exact relationship between the partition function for the DG model and the partition function for a 2d lattice coulomb gas. Using renormalization group methods (see Section VI for more details), Kosterlitz[44] had previously established that the coulomb gas has a phase transition from a low temperature dielectric fluid with opposite charges tightly bound together in "diatomic molecules" to a high temperature "metallic" phase with free charges and Debye screening. The properties of this transition can thus be directly related to those of the roughening transition. The DG-coulomb gas equivalence gave the first clear indication that the roughening transition has very different properties from those of the critical point in the 2d Ising model, which the simple argument of Burton, Cabrera, and Frank would associate with roughening.

The most dramatic differences show up in the behavior of the correlation length ξ. Define the height-difference correlation function

$$H(s - s') = \langle [h(s) - h(s')]^2 \rangle \tag{5.2}$$

where the brackets indicate an ensemble average in the DG (or SOS) system, and s and s' locate the centers of two columns. $H(s)$ gives a measure of the average fluctuations in height between different regions of the interface separated by a distance s, and the square of the *interface width* is the $s \to \infty$ asymptotic value of $H(s)$. The *correlation length* ξ is proportional to the separation s' at which $H(s)$ is approximately equal to its asymptotic value. Using Kosterlitz's results, Chui and Weeks showed that below T_R the interface width is finite with a finite correlation length ξ. At all temperatures above T_R, however, the interface width diverges as $s \to \infty$, and the correlation length ξ is infinite. For all $T \geq T_R$, $H(s)$ is proportional to ln s at large separations s, so the interface width diverges logarithmically.

Kosterlitz[44] further showed that the correlation length ξ diverges very rapidly as $T \to T_R$ from below:

$$\xi \propto \exp[c/(T_R - T)^{1/2}] \tag{5.3}$$

and of course ξ remains infinite for $T > T_R$. This behavior is very different from that of the 2d Ising model where ξ diverges by a power law only at T_c. Further, the free energy has a similar form near T_R

$$F \propto \exp\left[-\frac{c'}{(|T - T_R|)^{1/2}}\right] \tag{5.4}$$

The free energy is nonanalytic at T_R, but the singularity is a very weak one, with all temperature derivatives of the singular part vanishing at T_R. Thus the roughening transition is an infinite order transition. In particular, there is no anomaly in the specific heat at T_R, again differing from the Ising model result.

As discussed before, we expect this kind of behavior to apply to a wide class of interfacial models with different interaction energies between columns. Indeed, the work of Chui and Weeks strongly suggests that the restriction of the heights of the columns to be discrete integers is not important. A model that allows continuous height variables, but has a term in the Hamiltonian energetically favoring the integer positions should have the same behavior as the discrete models. See Section VI for an analysis of the dynamics of such a model. In the static limit it indeed reproduces the static behavior of the DG model.

Phase transitions in other models can also be related to the roughening

transition. Using physically plausible arguments, Kosterlitz and Thouless[44] had previously established a connection between the coulomb gas transition and a phase transition in the XY model (a model of two component spins which can rotate in the plane of the 2d lattice with an interaction energy proportional to $\cos\theta$, with θ the difference in angle between nearest neighbor spins). Hence the roughening transition is also related to the transition in the XY model. Recent work by José et al.[45] and Knops[12] have made this connection quite explicit mathematically. They have shown that a generalized SOS model with arbitrary interaction energy between nearest-neighbor columns can be related by an exact "duality transformation" to a generalized XY model in which the spin-spin interaction is some function $f(\theta)$ of the difference of angles. Presumably all these generalized XY models (for which $f(\theta)$ is analytic near $\theta = 0$) have the same behavior at their transition points.

Finally, van Beijeren[11] has established a direct connection between the *exactly solvable* six-vertex model[46] and a model for the roughening transition of the (001) face of a face-centered cubic crystal. In van Beijeren's model, the columns are perpendicular to the (001) plane, and the height of a column can differ by at most one unit from the height of the columns representing the nearest neighbor sites. Thus multiple height excitations of nearest neighbors are rigorously excluded. On physical grounds, we expect this exclusion to have no effect on the behavior at the roughening point. (van Beijeren actually considered a body-centered cubic model with second neighbor forces, but his results also apply to the face-centered cubic model with nearest-neighbor forces. We feel this interpretation is more physically appealing.)

The equivalence of this roughening model and the six-vertex model is important since the existence of the transition and many of its properties can be rigorously established.[46] The properties of the transitions in the XY model and the coulomb gas system have been analyzed by a renormalization group method which gives a very plausible but not completely rigorous description. Thus it is significant that the results of the renormalization group analysis for the XY and coulomb systems appear to be in complete agreement with the exact results of the six-vertex model. In particular, the free energy singularity in the six-vertex model is the same as that of (5.4). The correlation function $H(s)$ in (5.2) goes as $\ln s$ above T_R. Further, van Beijeren[11] showed by an explicit calculation for his model that the edge energy of a step goes rigorously to zero as $T \to T_R$ vanishing as $\exp[-c/(T_R - T)^{1/2}]$. There is no divergence in the step specific heat. Swendsen[47] has further shown that the free energy to form a step can be rigorously related to the inverse of the correlation length. Thus these results also confirm the form (5.3) for the divergence of the correlation length.

In summary, generalized SOS models which assign different energies to multiple height excitations can be exactly related to the 2d coulomb gas, the generalized XY model, and the six-vertex model. All of these systems seem to have the same behavior near the phase transition point, in agreement with our physical picture that multiple height excitations are unimportant at the roughening point. The theories confirm the divergence of the interface width, the vanishing of the edge free energy of a step, and other properties suggested by the MC and series expansion results. They provide the precise form of the behavior of these quantities as the roughening temperature is approached and show that the roughening transition has very different properties than does the one-layer model of the 2d Ising model at its critical point.

VI. DYNAMICS OF THE ROUGHENING TRANSITION

In this section we review a theory of crystal growth dynamics near the roughening point introduced by Chui and Weeks.[48] We are thus dealing with the interesting transition between sub-linear (nucleated) growth below T_R and continuous growth above. We assume that the reader has some familiarity with recent developments in the theory of dynamic critical phenomena.[49–51] The sections that follow can be read independently of this one.

We use ideas pioneered by Halperin, Hohenberg, and Ma[50,51] in their study of dynamics at the critical point. The situations are very similar; in both systems below T_R (T_c) there is a finite correlation length ξ which diverges as the roughening (critical) point is approached. However, the correlation length for all $T \geq T_R$ in the roughened phase remains infinite (as at a critical point), so the roughening point can be thought of as the low temperature end point of a line of critical points. As we saw in the previous section, the roughening point is very different from the critical point of an Ising model. Nonetheless, because the correlation length is very large compared to atomic spacings, we expect that many details of the microscopic Hamiltonian used to model the roughening transition are unimportant. Static calculations suggest, for example, that the precise form of the intercolumn interaction is unimportant, as is the restriction to discrete heights and lattice sites.[10] All such systems appear to lie in the same (static) universality class.

The fundamental idea in developing a tractable theory for dynamics at the roughening point is that of *dynamic universality*.[50,51] It is postulated that, in addition to all the properties that affect the static roughening behavior, one need consider in addition only the (hydrodynamic) conservation laws and couplings between the conserved variables. Details of the dynamics which do not affect conservation laws are irrelevant for a

description of the long-wavelength low-frequency behavior of the system at the roughening point. For example, systems with and without surface diffusion should exhibit similar behavior at their respective roughening transitions.

Our model for crystal growth is particularly simple, since there are no conserved quantities such as the energy or momentum density to consider. We have postulated from the first a stochastic and purely relaxational model of crystal growth. Assuming dynamic universality, we can thus study, for example, a simple relaxational Langevin model kinetic equation[51] ("Model A") and obtain information about all members of this universality class.

We consider the following generalized SOS model Hamiltonian for the crystal-vapor system

$$H=\frac{J}{2}\sum_{i,\delta}(h_i-h_{i+\delta})^2+Jg^2\sum_i h_i^2-\sum_i \Delta\mu_i h_i-2y_0J\sum_i\cos(2\pi h_i) \quad (6.1)$$

The first term gives the interaction energy between a column at site j (and height h_j) and its nearest neighbors at sites $j+\delta$; the second gives the interaction with a dimensionless "stabilizing field" g^2 which tends to localize the interface near $\langle h\rangle=0$. Usually we consider the limit $g^2\to 0^+$. The third term gives the interaction with "applied fields" $\Delta\mu_j$ which for generality can be different for different lattice sites. We later associate $\Delta\mu_j$ with the chemical potential driving force for crystal growth. The last term, parameterized by the dimensionless quantity y_0, is a *weighting function* which energetically favors integer values of the h_j. In the usual discrete lattice models, the weighting function is such as to permit only *integer values* of the h_j. Thus (6.1) can be looked on as a more general model in which continuous positions of the adatoms are permitted. Previous work indicates that any periodic weighting function will give the same static behavior at the roughening point.[10] This shows that the roughening phenomenon is not an artifact of the discrete lattice models assumed, but should also occur in more realistic models where atoms can move off their average lattice positions.

We introduce dynamics through the Langevin equation[51]

$$\frac{\partial h_j}{\partial t}=-\frac{\Gamma\delta H}{T\delta h_j}+\eta_j$$

$$=-\Gamma K^{-1}\sum_\delta(h_j-h_{j+\delta})-\Gamma K^{-1}g^2h_j+\Gamma(\Delta\mu_j/T)$$

$$-2\pi K^{-1}\Gamma y_0\sin 2\pi h_j+\eta_j \quad (6.2)$$

Here $K^{-1}=2J/T$. (We set Boltzmann's constant equal to unity in this section.) The η_j are Gaussain fluctuating white noises which satisfy

$$\langle\eta_j(t)\rangle=0$$

$$\langle\eta_j(t)\eta_{j'}(t')\rangle=2\Gamma\delta_{jj'}\delta(t-t') \quad (6.3)$$

where the angular brackets indicate an ensemble average. The parameter Γ is identified later with the equilibrium (kink-site) evaporation rate. We assume that the system starts from equilibrium at $t=-\infty$ and allow the applied fields $\Delta\mu_j$ to be time dependent.

If $y_0=0$, then (6.2) is a linear equation and can be solved exactly by Fourier transform methods in terms of a Green's function which, in the long wavelength limit, has the form[52]

$$G(q,\omega)=[K^{-1}(q^2+g^2)-i(\omega/\Gamma)]^{-1} \quad (6.4)$$

In the limit $g^2\to 0^+$, which we consider hereafter, G is the Green's function for 2d diffusion. This is not surprising, since when $y_0=0$, (6.2) is a finite difference analog of the diffusion equation.

For nonzero y_0, (6.2) can be written

$$h(s,t)=\int_{-\infty}^{\infty}ds'\int_{-\infty}^{\infty}dt'G(s-s',t-t')[\Delta\mu(s't')/T$$

$$+\eta(s't')/\Gamma-2\pi K^{-1}y_0\sin 2\pi h(s't')] \quad (6.5)$$

Here s is a dimensionless 2d lattice vector (the unit of length being the lattice spacing) locating the center of a column. We have taken the limit of an infinite system and replaced sums by integrals.

We analyze (6.5) using linear response theory, assuming that the driving force $\Delta\mu$ is infinitesimally small. Hence we try to predict the limiting slope of the growth rate curve as the driving force tends to zero. In addition, the linear response analysis gives valuable information about spatial and temporal correlations of the interface at equilibrium when $\Delta\mu=0$.[51,53]

Expanding the solution of (6.5) in powers of $\Delta\mu/T$,

$$h(s,t)=h_0(s,t)+\int ds'\int dt'h_1(st,s't')\frac{\Delta\mu(s't')}{T}+O\left(\frac{\Delta\mu}{T}\right)^2 \quad (6.6)$$

the linear response function $\chi(q,\omega)$ is given by the ensemble average over the noise

$$\chi(q,\omega)=\langle h_1(q,\omega)\rangle \quad (6.7)$$

and using (6.4) to (6.6), the unperturbed ($y_0=0$) response function explicitly is

$$\chi_0(q,\omega)=G(q,\omega)=[K^{-1}(q^2+g^2)-i(\omega/\Gamma)]^{-1} \quad (6.8)$$

The effect of a non-zero y_0 is conveniently expressed in terms of a self-energy $\sum(q, \omega)$, defined as

$$\chi^{-1}(q, \omega) = \chi_0^{-1}(q, \omega) + \sum(q, \omega) \tag{6.9}$$

Substituting (6.6) into (6.5), we find after some manipulation a formally exact expression for $\sum$ given by

$$\sum(q, \omega) = \frac{4\pi^2 y_0 K^{-1} F\{\langle \cos[2\pi h_0(st)] h_1(st, s't') \rangle\}}{\langle h_1(q, \omega) \rangle} \tag{6.10}$$

where $F\{\ \}$ denotes a Fourier transform in space and time. Note that the term transformed is a function only of the differences $s - s'$ and $t - t'$ since the noise ensemble is stationary.

The behavior of $\sum$ in the limit of very low temperatures is easy to analyze. The equilibrium fluctuations of h_0 are very small at low temperatures, and the weighting function localizes the interface very near $h_0 = 0$. Linearizing the sine term in (6.2) then gives a constant value for $\sum$ of

$$\sum(q, \omega) \cong 4\pi^2 y_0 K^{-1} \tag{6.11}$$

Thus from Eq. (6.9) there is a finite response even in the $q, \omega \to 0$ limits at low temperatures.

At high temperatures ($T > T_R$) the situation is very different. Here the weighting function has little effect on the system. Thermal fluctuations are large enough that the interface wanders arbitrarily far from its $T = 0$ location (this delocalization characterizes the roughened phase). When $y_0 = 0$, the weighting function vanishes altogether and the response function can be calculated exactly. This divergent response function [(6.8)] presumably gives the limiting high temperature behaviour of a system with a finite y_0.

These qualitative arguments can be put on a much firmer basis by using the renormalization group method of Kosterlitz[44] and José et al.[45] We consider an expansion of the inverse linear response function $\chi^{-1}(q, \omega)$ in powers of y_0. Similar expansions have proved very useful in the static limit.[45,54] The zeroth order term $[\chi_0^{-1}(q, \omega)]$ gives the limiting ($T \to \infty$) behavior, and the higher-order terms give corrections arising from a nonzero weighting function. We use this expansion to derive differential *recursion relations* which relate the response in the original system with parameters K, Γ, and y_0 to that in a system with renormalized parameters K', Γ', and y_0'. Integration of the recursion relations in fact provides a connection for all $T \geq T_R$ between the original system and the exactly solvable system with $y_0 = 0$.

Expanding h_0, h_1, and $\sum$ in powers of y_0, we find, using (6.5) to (6.10), after some straightforward but tedious algebra (much of which can be found in an article by de Gennes[52]), that (6.9) can be written to lowest order in q and ω as

$$\chi^{-1}(q, \omega) = \left[K^{-1} + \pi^3 K^{-2} y^2 \int_1^\infty ds\, s^{3-2\pi K}\right] q^2 - i\omega\left[\Gamma^{-1} + \Gamma^{-1} \frac{\pi^4 y^2}{(\pi K - 1)} \int_1^\infty ds\, s^{3-2\pi K}\right] + O(y^4) \tag{6.12}$$

where $y \equiv y_0 \exp[-Kc]$ and c is a constant approximately equal to $\frac{1}{2}\pi^2$. Now divide the range of integration of each integral in (6.12) into two parts: 1 to b and b to ∞, with $0 < \ln b \ll 1$ (i.e., b is very close to unity). The small s parts of the integration can be combined with the original constant term (either K^{-1} or Γ^{-1}) to yield a new parameter value and the large s part of the integration rescaled so that the integrals again run from 1 to ∞. The scale factor is absorbed in a redefined y variable. Equation 6.12 can thus be rewritten in exactly the same functional form with K, y, and Γ replaced by $K(l)$, $y(l)$, and $\Gamma(l)$, with $l \equiv \ln b$. This equivalence implies the differential recursion relations

$$\frac{dK(l)}{dl} = -\pi^3 y^2(l) \tag{6.13}$$

$$\frac{1}{2}\frac{dy^2(l)}{dl} = -[\pi K(l) - 2] y^2(l) \tag{6.14}$$

$$\frac{d \ln \Gamma(l)}{dl} = -\frac{\pi^4 y^2(l)}{\pi K(l) - 1} \tag{6.15}$$

subject to the boundary conditions $K(l = 0) = K$, and so on.

The first two equations are essentially identical with the static recursion relations found by José et al.[45] and Nelson and Kosterlitz[54] in their analyses of the planar XY model and the 2d coulomb gas. This shows that the static behavior at the roughening transition is the same as that of the XY and coulomb gas systems at their transition points. It is easy to show by integrating these equations that $y(l)$ is driven to zero as $l \to \infty$ for all temperatures greater than the roughening temperature. This provides a justification for the original expansion in powers of y_0. The roughening temperature can thus be thought of as the low temperature end point of a fixed line of "critical" points where $y(\infty) = 0$. For all $T \geq T_R$, the correlations in the original system with nonzero y_0 can be described in terms of the divergent response function $\chi_0(q, \omega)$, with renormalized values of the parameters K and (as shown below) Γ.

The third equation describes the behavior of the dynamical parameter Γ. Eliminating $y^2(l)$ between (6.13) and (6.15) and integrating from $l = 0$

to $l=\infty$, we have

$$\frac{\Gamma(\infty)}{\Gamma}=\frac{\pi K(\infty)-1}{\pi K-1} \tag{6.16}$$

Here $\Gamma(\infty)$ and $K(\infty)$ are the renormalized values of the bare parameters Γ and K. Thus Γ effectively scales with K, whose behavior has already been discussed by Kosterlitz[44] and José et al.[45] For example, it is easy to show from (6.14) that $K(\infty)=2/\pi$ at the roughening temperature. Equation 6.16 shows that the renormalized Γ is reduced from its bare value, but does not vanish along the entire fixed line of critical points which characterizes the roughened phase including the end point at T_R. Using the language of Hohenberg and Halperin,[51] the dynamics is thus *conventional*. However, the mutual scaling of K and Γ represents an interesting and somewhat unconventional feature of the model. The static calculations have shown that $K(\infty)$ has a square root cusp[44,54] as $T\to T_R$; thus it should be possible to observe a similar anomaly in $\Gamma(\infty)$.

These results have several immediate consequences for the static and dynamic behavior of the crystal-vapor interface. For example, the average growth rate R of a crystal is related to the response to a spatially and temporally uniform driving force when the stabilizing field $g^2=0$. To first order in $\Delta\mu$ it is given by

$$R=\lim_{\omega\to 0}-i\omega\chi(q=0,\omega)\frac{\Delta\mu}{T} \tag{6.17}$$

$$=\Gamma(\infty)\frac{\Delta\mu}{T}\qquad (T\geq T_R) \tag{6.18}$$

Thus the theory predicts linear growth at and above T_R in agreement with conventional theories of crystal growth. In particular, note from (3.12) that the Wilson-Frenkel high temperature limiting growth law can be written to first order in $\Delta\mu$ as

$$R_{WF}=k_{eq}\frac{\Delta\mu}{T} \tag{6.19}$$

At very high temperatures, the bare and renormalized parameters become equal. Thus we can identify Γ with the equilibrium evaporation rate k_{eq}. Equation 6.18 then provides an expression for the limiting slope of the growth rate curve at lower temperatures in the continuous growth regime ($T>T_R$).

Below T_R, the situation is very different. Approaching the roughening temperature from below, the response function has the limiting form

$$\chi(q,\omega)=[K'(q^2+\xi^{-2})-i(\omega/\Gamma')]^{-1} \tag{6.20}$$

with a finite correlation length ξ and renormalized coefficients K' and Γ'. Equation 6.17 then predicts a zero growth rate for $T<T_R$ to first order in $\Delta\mu/T$. This result is consistent with the fact that growth at low temperatures occurs by a nucleation mechanism. Nucleation theory gives the result $R\propto\exp(-c/\Delta\mu)$ [see (4.22)], so in fact below T_R all terms in a power series about $\Delta\mu=0$ should vanish.

This change in growth mechanism is directly related to the change in the *equilibrium* spatial and temporal correlations between different parts of the interface. The height-height correlation function can be immediately calculated from the fluctuation-dissipation theorem[53]

$$\langle|h_0(q,\omega)|^2\rangle=\frac{2}{\omega}\,\mathrm{Im}\,[\chi(q,\omega)] \tag{6.21}$$

where Im [ ] denotes the imaginary part. In particular, for $T\geq T_R$ and large s or large t,

$$\langle[h_0(s,t)-h_0(0,0)]^2\rangle\cong\frac{K(\infty)}{2\pi}\ln\left\{\max\left[s^2,\frac{4\Gamma(\infty)}{K(\infty)}t\right]\right\} \tag{6.22}$$

where we have used some results of de Gennes.[52] Thus there are logarithmically diverging correlations in space and time above T_R. The large distance limiting value of the equal time correlation function gives a measure of the interface width. Equation 6.22 shows that the interface width diverges logarithmically for all $T\geq T_R$. Similar remarks apply to the temporal correlations. Equation 6.22 also implies that the correlation length ξ is infinite for all $T\geq T_R$.

Below T_R, (6.20) holds and the correlation functions reaches *finite* asymptotic values exponentially fast. In particular, the interface width is finite below T_R, and there is a finite correlation length. There are many other interesting features of the roughening point that follow from a more careful analysis of the renormalization group equations. Most of these are mentioned in the preceding section.

Many of these predictions can be checked by currently available computer simulation methods. For example, we can use (6.22) to provide an important quantitative test of the theory. As mentioned before, at the roughening point $K(\infty)=2/\pi$. Equation 6.22 then predicts for the equal time height-height correlation function at the roughening temperature

$$\langle[h_0(s)-h_0(0)]^2\rangle\cong\frac{2}{\pi^2}\ln s \tag{6.23}$$

Shugard et al. have provided MC simulations of this correlation function for the solid-on-solid model[9] and indeed find a logarithmic correlation function dependence with a coefficient very nearly $2/\pi^2$ at the roughening

point. This agreement strengthens our confidence in the general approach taken here, and in particular the ideas of static and dynamic universality that underly the method.

VII. SPIRAL GROWTH AND THE INFLUENCE OF LINE DEFECTS

The previous sections have been concerned with the properties of low index faces on perfect crystals. This is essential for an understanding of the crystal growth process. Because of the slower kinetics of the low index faces, the morphology of the growing crystal usually consists of a polyhedron bounded with these faces. However, real crystals normally contain impurities and lattice defects such as screw dislocations, and these can have a tremendous effect on the growth kinetics. In 1931 Volmer and Schultz[55] observed iodine crystals growing from the vapor and measured growth rates that were a factor of exp (1000) larger than the prediction of 2d nucleation theory! In the following sections we discuss the relation between defects or impurities and crystal growth kinetics. Much of the quantitative data is obtained by the MC technique, especially in the more complex situations in which several mechanisms contribute to the growth process.

A. Screw Dislocations

The importance of dislocations in crystal growth was first pointed out by Frank,[56] who realized that they could enhance the growth rate of low index faces by many orders of magnitude. A dislocation that terminates with a component of its Burger's vector perpendicular to the surface circumvents the difficult process of nucleating new layers. The step that is connected with this dislocation can wind up into a spiral and thereby provide a continuous source of edge positions. The nucleation of 2d clusters is unnecessary. Dislocations are especially important at low temperatures and driving forces, where the growth rate of a perfect crystal face is essentially zero. Many aspects of the spiral growth process have not been investigated. Vapor deposition experiments are usually performed in the presence of a large driving force, and 2d nucleation can proceed at an appreciable rate. The importance of dislocations is open to question in this case. Also, the relation between dislocations and hillocks on vapor-grown crystals requires consideration.

The formation of a spiral step pattern around a screw dislocation is illustrated in Fig. 12. The temperature is indicated by the ratio L/kT, where L is the binding energy per atom in the lattice. This ratio has proved to be useful for comparisons with real crystals.[39] In the SC lattice

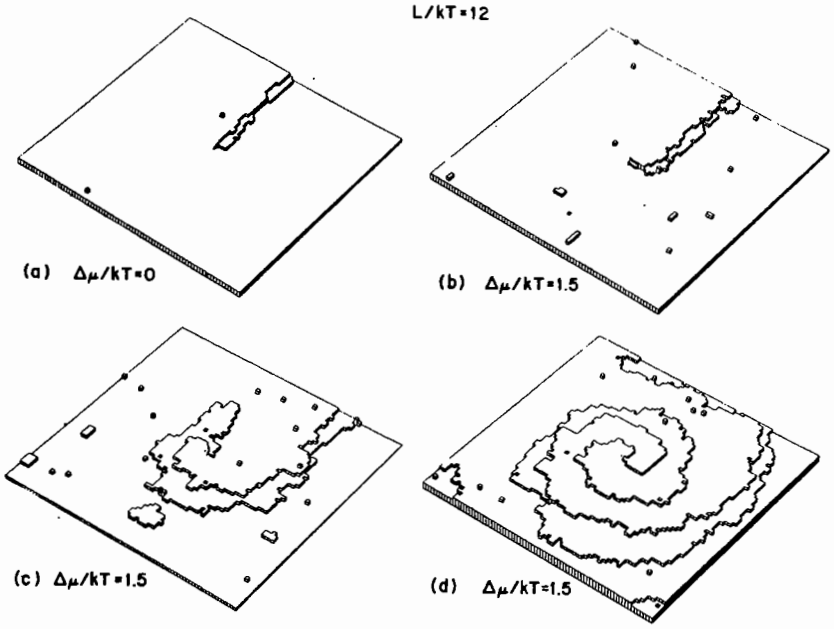

Fig. 12. An illustration of the formation of a double spiral. (a) is an equilibrium configuration, whereas (b) to (d) illustrate the step motion resulting from a driving force of $\Delta\mu = 1.5kT$.

$L = 3\phi$, and hence $L/kT = 12$ corresponds to $kT/\phi = 0.25$, that is, a temperature less than half T_R. These drawings correspond to configurations generated during a MC simulation. The screw dislocation intersects the surface at the center of the section illustrated. The magnitude of the Burger's vector is two, as indicated by the two associated steps. The steps are pinned at the dislocation, but a finite driving force causes them to advance along most of their length. The steps tend to separate from one another both in equilibrium and during growth. This is a consequence of the fact that it is energetically very unfavorable for steps to cross or overlap one another at any point. (The SOS model "no overhang" restriction rules out crossings entirely.)

A segment of the step at the upper level does occasionally move up so that it coincides with the lower step, but atoms impinging at the edge of this segment cause only the lower step to advance, and it then moves ahead of the upper step. This "kinetic repulsion"[57] between neighboring steps tends to produce a stable pattern of separated steps. Since one of the ends is pinned, the steps associated with the screw dislocation eventually assume an irregular spiral pattern that extends over the entire

crystal face. The spiral emanating from a single dislocation can provide a uniform distribution of edge sites over faces of macroscopic dimensions, although a very long transient period would be required before steady-state conditions obtain. The spiral step pattern simply rotates about the position of the dislocation as growth proceeds and provides an inexhaustible source of edge positions where impinging atoms may attach to the crystal.

Polygonized spirals may occur at low temperatures when the free energy of a step is sensitive to its orientation.[22] Theories for the kinetics of polygonized spirals are in the literature,[58,59] and for simplicity we limit our consideration to steps with a high density of kink sites and rounded spirals.

The presence of screw dislocations permits measurable growth to occur on close-packed faces under conditions in which the 2d nucleation rate is infinitesimal. The actual growth rate depends on the average distance l between the arms of the spiral steps far from the source. Cabrera and Levine[60] calculated l in the case in which the step could be approximated by a smooth spiral curve. Surface migration and 2d nucleation were excluded in this treatment. Anisotropy of the step free energy was also neglected. The average velocity of a step segment is related to its radius of curvature ρ through the equation

$$v_\perp = v_\infty(1-\rho_c/\rho) \tag{7.1}$$

where $v_\perp$ is the velocity measured in a direction perpendicular to the segment, ρ_c is the radius of the critical nucleus, and v_∞ is the velocity a straight step. Equation 7.1 includes the first-order correction (in ρ^{-1}) for the curvature of the step. This accounts for the fact that atoms at the edge of the curved step have fewer neighbors and are more likely to evaporate than those along the edge of a straight step. Atoms at the edge of a step with the curvature of the critical nucleus are equally likely to grow or evaporate. Hence, (7.1) is correct when $\rho = \rho_c$, and it is probably accurate for larger values of ρ provided $\rho_c \gg a$.

Apparently there is a unique spiral form that rotates around the screw dislocation without changing shape. The curvature of the step at the point where it is pinned to the dislocation is assumed to be ρ_c, since this point does not move. Dimensional arguments indicate that the asymptotic spacing l between adjacent arms is proportional to ρ_c, and $l = 19\rho_c$ according to the series solution of Ref. 60. The crystal growth rate normal to the close-packed surface is inversely proportional to l, that is,

$$R = \frac{v_\infty a}{l} = K\frac{v_\infty \Delta\mu}{\phi} \tag{7.2}$$

The critical nucleus size $i^* = (\phi/\Delta\mu)^2$ (see Section IV) is employed in the second equality to evaluate ρ_c, and $K \cong 0.1$ is a dimensionless constant determined by the ratio ρ_c/l and the geometry of the cluster.[60] At high temperatures, ϕ must be replaced by 2γ, where γ is the edge free energy per interatomic spacing along the step.

Equation 7.2 predicts a parabolic dependence of R on $\Delta\mu$ in the regime where $v_\infty \propto \Delta\mu$. However, the growth rate on a perfect crystal face in (4.22) contains $\Delta\mu$ in the denominator of a negative exponent, and hence this expression is much smaller than (7.2) in the limit as $\Delta\mu \to 0$. Neither (4.22) nor (7.2) is accurate at large driving force, and the analytical models can not determine which mechanism is the dominant mode of crystal growth in this regime.

MC calculations of growth rates on crystal faces with a screw dislocation are shown in Fig. 13 (closed symbols). 2d nucleation is also possible, and both mechanisms may contribute to the total growth rates measured. Surface migration is excluded. For comparison, the growth rates of perfect crystal faces are also plotted (open symbols). At $L/kT = 6$ ($kT/\phi = 0.5$) dislocations have little effect, even though a Burger's vector of four was used to enhance the difference between the two rates. Very precise data near the origin does reveal significant differences, since the temperature is slightly below the roughening point and a small nucleation barrier is present.

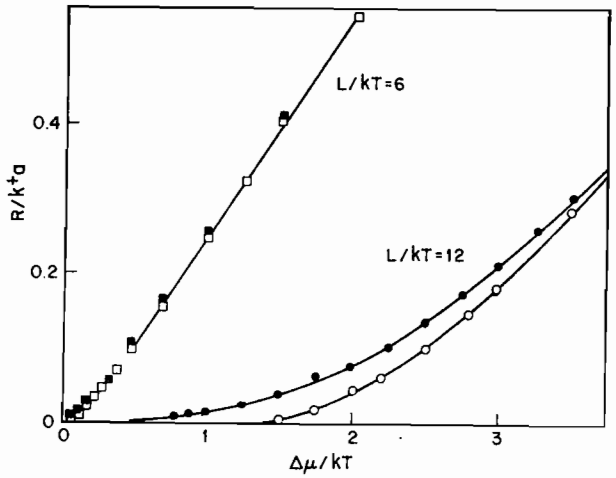

Fig. 13. MC calculations of growth on a perfect crystal and of spiral growth are compared (open and closed symbols, respectively).

The screw dislocations have a large effect on the growth kinetics at $L/kT = 12$. Finite growth rates are observed with $\Delta\mu < kT$, a region in which the perfect surface is essentially static. The relative increase in the growth rate diminishes as $\Delta\mu$ increases, and for $\Delta\mu > 3kT$ the 2d nucleation rate is so large that the additional steps afforded by the screw dislocation have little influence. (In this case a Burger's vector of two was used.)

These results suggest that the surface of a crystal containing a screw dislocation always grows faster than that of a perfect crystal. This is not surprising, since the presence of the extra steps associated with a screw dislocation provide more growth sites than 2d nucleation alone on a perfect crystal surface. Nucleation can occur in parallel with spiral growth; and this is apparent in Fig. 12 where a large cluster is present some distance away from the steps. The increase in the growth rate caused by screw dislocations varies from a fraction of a percent at high temperatures and large $\Delta\mu$ to many orders of magnitude at the opposite extreme.

The spiral growth rate without 2d nucleation can also be measured by the MC method. A special simulation of spiral growth is required in which the 2d nucleation of clusters is suppressed. This is accomplished by inhibiting the deposition of atoms on sites where they would have only one bond to the crystal, that is, $k_1^+ = 0$. (In this and the following sections it is convenient to change the notation to indicate the total coordination number of an atom; e.g., an adatom evaporation rate is k_1^-. Previously k_1^- referred to the evaporation rate of an atom with one *lateral* bond and a coordination number of two.) This does not directly affect the motion of steps, since the sites at the step edge would afford at least two bonds to impinging atoms, but it does prevent the nucleation of clusters that start as single adatoms. (It is also necessary to suppress the annihilation of any one-bonded atoms that are formed by other processes, since the transition probabilities must satisfy microscopic reversibility in equilibrium.)

The growth rate of the crystal with a screw dislocation and $k_1^+ = 0$ is plotted in Fig. 14 (open triangles), together with corresponding data from Fig. 4. The spiral growth rate at values of $\Delta\mu < 2kT$ is not noticeably perturbed by the nucleation of clusters, even though the perfect crystal growth rate is about half the spiral growth rate at $\Delta\mu = 2kT$. At larger values of $\Delta\mu$, nucleation does produce an appreciable increase in the growth rate. Note that the nucleation and spiral growth processes contribute to the combined growth rate in a highly nonlinear fashion, the sum of the two rates being larger than the combined rate. This is to be expected, since 2d clusters and steps interact in a complex way and some clusters may be incorporated into an advancing step at an early stage and contribute little to the process of crystal growth.

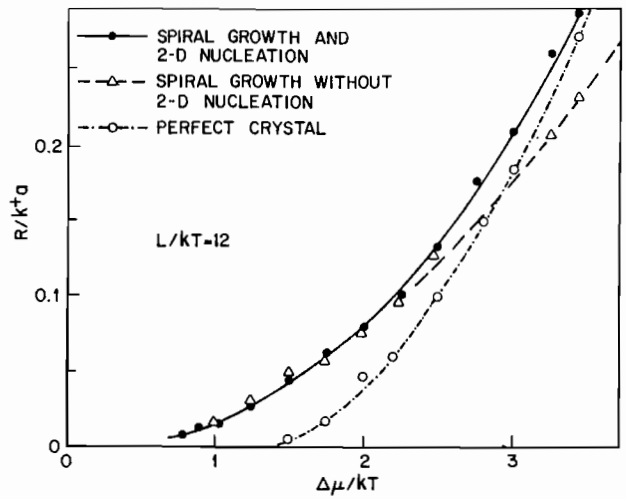

Fig. 14. Normalized growth rates of a surface intersected by a screw dislocation, with and without 2*d* nucleation. The growth rates of a perfect crystal are included for comparison. Here $\beta\phi = 4$.

These data illustrate an important advantage of the MC method over the more idealized analytical models: complex situations can be treated on a quantitative basis. Much experimental data has been expressed in the form

$$R = A(\Delta\mu)^n \tag{7.3}$$

where n is usually an irrational number greater than unity. A least-squares fit to a plot of $\ln(R)$ versus $\ln(\Delta\mu)$ yields a value $n = 2.00 \pm 0.05$ in the case where $k_1^+ = 0$ (see also Ref. 59). The data of Fig. 14 correspond to a value of $n = 2.17 \pm 0.05$; the contribution of nucleation at large values of $\Delta\mu$ induces a steeper average slope in the plot. This indicates that irrational values of n may occur when several mechanisms operate in the range of driving force that is investigated.

The presence of surface diffusion does not change the fundamentals of spiral growth. The one complication that arises is the competition between adjacent arms of the spiral for the adatom flux. At small values of $\Delta\mu$ adjacent arms may be farther apart than the mean diffusion distance of an adatom along the surface. In this case, the mobility of the adatoms simply increases the value of v_∞, and (7.2) is still valid. At larger values of the driving force the growth rate is reduced by competition, and (7.2) is not applicable in this region.[61]

The value of v_∞ for an isolated step with surface migration can be calculated analytically. We assume for simplicity that the step is perfectly

straight, infinitely long, and parallel to a ⟨100⟩ direction. We also assume that the average evaporation rate is k_3^- per edge atom in the step. This is equivalent to the Wilson-Frenkel law discussed in Section III. It is accurate over a much wider range of temperatures and surface mobilities when applied to steps because the edge of a step is more disordered than the close-packed face. The flux of atoms per site to the edge of the step resulting from direct impingement and evaporation is

$$Q_0 = k^+ - k_3^- \tag{7.4}$$

In addition, we must include the flux resulting from the migration of atoms to and from the step.

The probabilities c_j of finding adatoms on sites j units from the edge of the step are related by the set of conservation equations

$$dc_j/dt = k^+ + \tfrac{3}{8}k_{11}(c_{j+1}+c_{j-1}) - \tfrac{3}{4}k_{11}c_j - k_1^- c_j \tag{7.5}$$

The first term on the right corresponds to addition by direct impingement on the site, and the second accounts for a migration to the site of an atom in an adjacent row. Here k_{11} is the adatom migration rate. The factor $\frac{3}{8}$ appears, since only three of the eight possible migration jumps would move an atom from row $j+1$ to row j, for example. (The simulation permits direct jumps to all eight sites that surround the migrating atom.) The third term accounts for migration from the site, and the factor $\frac{3}{4}$ is required, since only six of the eight jumps remove an atom from row j. Finally, $k_1^- c_j$ is the evaporation rate from the site. Note that we neglect any clustering of adatoms in this formulation.

In the steady state, $dc_j/dt = 0$, and (7.5) is satisfied by an expression of the form

$$c_j = (k^+/k_1^-)(1 - Ae^{-\lambda j}) \tag{7.6}$$

where A and λ are constants. Substitution of (7.6) into (7.5) yields

$$\lambda = 2\ln[(\tfrac{2}{3}k_1^-/k_{11})^{1/2} + (\tfrac{2}{3}k_1^-/k_{11}+1)^{1/2}] \tag{7.7}$$

The concentration c_1 at a site one unit removed from the edge of the step obeys the relation

$$dc_1/dt = k^+ + \tfrac{3}{8}k_{11}(c_2 + k_3^-/k_1^-) - \tfrac{3}{4}k_{11}c_1 - k_1^- c_1 \tag{7.8}$$

This equation is identical to (7.5) with $j = 1$, except for the replacement of c_0 in (7.5) by k_3^-/k_1^-, the equilibrium density of adatoms. This is consistent with the previous assumption that the average evaporation rate from the sites at the edge of the step is the equilibrium rate. Substitution of (7.6) into the steady-state form of (7.8) yields

$$A = (1 - k_3^-/k^+)/[2e^{-\lambda} + \tfrac{8}{3}(k_1^-/k_{11})e^{-\lambda} - e^{-2\lambda}] \tag{7.9}$$

The surface flux to the step results from the exchange between the atoms in the edge of the step and the adatoms in the adjacent row of sites; that is,

$$\begin{aligned} Q_s &= \tfrac{3}{8}k_{11}(c_1 - c_0) \\ &= \tfrac{3}{8}(k_{11}/k_1^-)[(k^+ - k_3^-) - k^+ Ae^{-\lambda}] \end{aligned} \tag{7.10}$$

where c_1 is eliminated in the expression on the right by the use of (7.6). Equations 7.7 and 7.9 provide the needed expressions for A and λ, and after some manipulation we achieve the simple result

$$Q_s = (k^+ - k_3^-)[(\tfrac{1}{4} + \tfrac{3}{8}k_{11}/k_1^-)^{1/2} - \tfrac{1}{2}] \tag{7.11}$$

The velocity of the step is a result of direct impingement and migration of adatoms to *both* sides, since in this theory, as in the MC model, adatoms are allowed to jump to sites at different levels. Thus

$$\begin{aligned} v_\infty &= a(Q_0 + 2Q_s) \\ &= ak^+[1 - \exp(-\Delta\mu/kT)](1 + \tfrac{3}{2}k_{11}/k_1^-)^{1/2} \end{aligned} \tag{7.12}$$

Figure 15 is a plot of spiral and perfect crystal growth rates, both calculated in the presence of surface migration. The dashed curves indicate the growth rates calculated without surface migration. The ratio

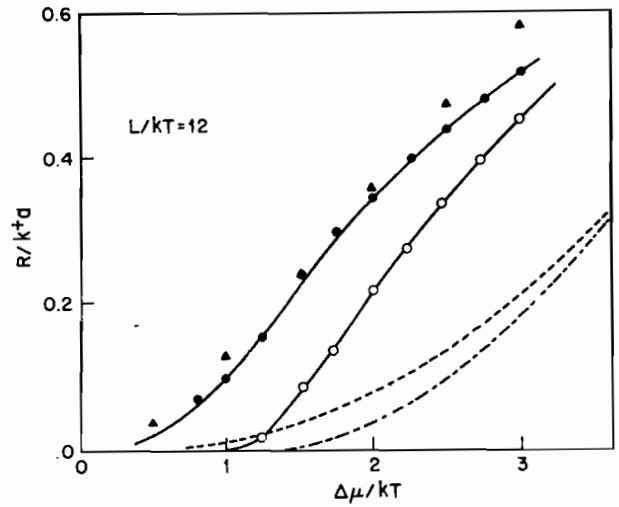

Fig. 15. Spiral and perfect crystal growth rates (closed and open circles) calculated with a surface migration to evaporation ratio of 7.4. The triangles represent the spiral growth rate calculated with (7.2) and (7.12). The dashed curves indicate the growth rates calculated without surface migration.

of the migration to evaporation rate is $k_{11}/k_1 = 7.4$ at the indicated temperature. The spiral growth rate derived from (7.12) and (7.2) is indicated by the triangles. The competition between adjacent arms of the spiral for the surface migration flux was neglected in the derivation of (7.12), and this is an important factor at larger values of $\Delta\mu$ where the arms are closely spaced.[61]

The agreement between theory and the MC data at small $\Delta\mu$ values contrasts with the observation, in the absence of surface diffusion, that the theoretical growth rates were about a factor of two larger than those calculated by the MC method.[6] The reason for the better agreement is related to the evaporation rate for atoms at the edge of the step. The actual evaporation rate during growth is generally higher than the equilibrium value, since the larger impingement rate causes some extra roughening of the step edges. Migration along the edge of the step tends to reduce this effect in a similar fashion to that described in Section III for crystal surfaces. In this case there is sufficient mobility of the atoms in the edge to maintain an evaporation rate close to the equilibrium value. According to the MC data, the addition of surface diffusion causes about a sixfold increase in the growth rate at low values of $\Delta\mu$. The increase that results from adatom diffusion to the step is ~3.5 according to the analysis above. The reduction in the evaporation rate from the step edges must account for the remaining increase. Gilmer and Bennema[62] simulated the growth of stepped surfaces at $L/kT = 6$ with and without surface migration, and in this case adatom diffusion to the steps fully accounts for the increase in the growth rate. At this temperature the edge evaporation rate is approximately k_3^-, even in the absence of surface migration.

The spiral step(s) around a screw dislocation appear as a hillock on the crystal surface when viewed on a macroscopic scale. Hillocks with steep sides may affect the performance of semiconductor devices, for example, and an important practical problem is to find conditions for growth that minimize this effect.[63] The slope of the hillock surrounding the screw dislocation of the MC model is plotted in Fig. 16. The triangles indicate the average slope during steady-state growth. The slope predicted by Cabrera and Levine[60] is indicated by the dashed line. The theory is in good agreement with the data, even at the larger values of $\Delta\mu$ where the screw dislocation has little effect on the kinetics of growth. Large fluctuations in slope are observed in this region however, and these data are less reliable. The open circles represent data on a model that includes surface migration. Although these points can not be distinguished from the other data at small $\Delta\mu$, there is some evidence that surface mobility reduces the slope at large $\Delta\mu$, as expected. Again, this is a result of competition between adjacent arms of the spiral for the adatom flux.[61,64] Thus it

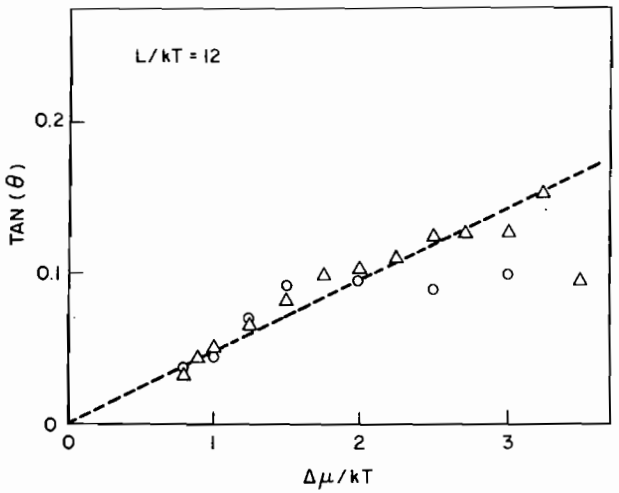

Fig. 16. The average slope of the hillock around a screw dislocation with $b = 2$. The triangles and dashed line indicate the MC data in the absence of surface migration, whereas the circles indicate data taken when the adatom jump rate is ~7.4 times the evaporation rate.

appears that the smallest slopes occur on crystals that are grown at small values of $\Delta\mu$ or that have a large surface mobility. There is little or no reduction in the slope when $\Delta\mu$ is increased to the point at which 2d nucleation becomes operative.

B. Asymmetry Between Crystal Growth and Evaporation

The crystal growth mechanisms described in this and the previous sections can also operate during evaporation. Evaporation (dissolution or melting) of crystal lattice planes occurs when the chemical potential is less than the equilibrium value, or $\Delta\mu < 0$. The nucleation of 2d holes in a close-packed surface layer proceeds by the evaporation of single atoms to form surface vacancies, then divacancies, and so forth until a stable cluster of vacant sites is formed. This process is exactly analogous to the nucleation of 2d clusters during growth. Evaporation by a spiral mechanism may also occur. Atoms at the edges of steps that are associated with screw dislocations tend to evaporate preferentially. Here too the steps wind into a spiral pattern, but in the opposite sense to the growth spiral. Thus one might expect the evaporation rate of a crystal at a negative chemical potential $\Delta\mu$ to be equal in magnitude to the growth rate at the positive value $|\Delta\mu|$. However, most experimental evaporation rates are much greater than the corresponding growth rates. The explanation of

this asymmetry between growth and evaporation is related to another kind of defect in the crystal lattice.

Edge dislocations are not accompanied by step segments on the surface, and they have only a small influence on the crystal growth rate. The nucleation of new lattice planes is not facilitated by the presence of these defects. In fact, a high density of dislocations may cause a small reduction in the crystal growth rate. This reduction occurs when the strain energy of the dislocations and the lower density of the imperfect crystal lattice produce a significant decrease in the binding energy of the atoms to the crystal.

On the other hand, the rate of evaporation is increased when edge dislocations are present. Part of this increase is simply the direct result of the reduced binding energy per atom in the crystal. However, the core of the dislocation with its high concentration of strain energy may have a more important effect. It can serve as a very efficient site for the 2d nucleation of holes. The reduced nucleation barrier at this point often causes a dramatic change in the evaporation rate of the crystal. Small voids and inclusions are commonly observed in crystals, and these should also reduce the growth rate and increase the evaporation rate.

Figure 17 is a plot of MC calculations of the net rate of gain (or loss) of material by a crystal with a line defect.[65] As in the previous case, $L/kT = 12$. This defect is a small (5×5) columnar hole that lies perpendicular to the (001) face on which the impingement and evaporation events are simulated. The growth rates are indistinguishable from those of the perfect crystal (see Fig. 4). The evaporation rate is appreciable even at $\Delta\mu = -kT$, whereas the growth rate is too small to measure at $\Delta\mu = kT$.

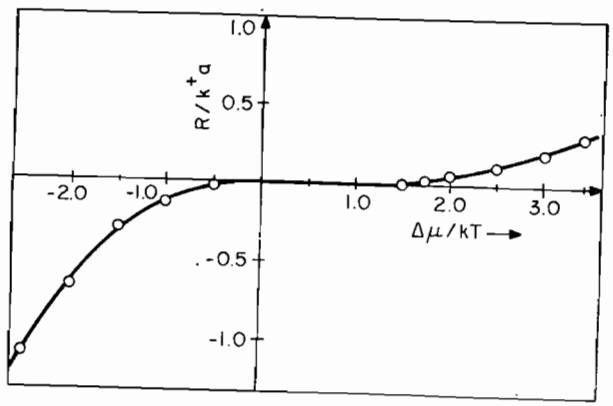

Fig. 17. Growth and evaporation rates of a crystal surface intersected by a columnar 5×5 hole. Here $L/kT = 12$.

It should be noted that the impingement and evaporation rate constants are not symmetric, and this has some effect on the symmetry of the kinetics illustrated here. For example, the formation of a surface vacancy requires the evaporation of a five-bonded atom. This is much slower than the rate of condensation of adatoms by direct impingement, which at equilibrium is equal to the evaporation rate of a three-bonded atom. This asymmetry favors the crystal growth process, but the growth rate in Fig. 17 is normalized by k^+, and the effect of this term is to increase the magnitude of the plotted values of the evaporation rate. These two effects tend to cancel one another, and normalized growth and evaporation curves for perfect crystal faces are approximately symmetrical over a wide range of $\Delta\mu$ values.[62]

The evaporation rate as represented in Fig. 17 is highly nonlinear, and there is a small region $(-0.5 < \beta\Delta\mu < 0)$ where the rate is essentially zero. The columnar hole in the crystal represents a cluster of 25 vacant sites in each layer, but in this region of $\Delta\mu$ they do not constitute a critical cluster. The classical expression for the number of atoms in a critical cluster, $i^* = (\phi/\Delta\mu)^2$, applies also to vacancy clusters when $\Delta\mu$ is negative. According to this expression, the critical hole contains 25 vacancies when $\beta\Delta\mu = -0.8$. We would therefore expect a rapid increase in the evaporation rate in the vicinity of this value, as is observed in Fig. 17.

Exposed atoms at the edge of the 5×5 hole readily evaporate at large negative values of $\Delta\mu$, that is, $\beta\Delta\mu \ll -0.8$. As the edge atoms of one layer evaporate, those of the layer below are exposed and soon evaporate also. In this way, an etch pit with steep sides is formed around the hole. This is illustrated in Fig. 18, where $\beta\Delta\mu = -2$. At values of $\Delta\mu$ closer to zero, the enlargement of the hole involves a nucleation event, and only a very shallow pit is formed.

The slope of the etch pit can be calculated from the evaporation rate R_e of the crystal. The growth rate of a vicinal surface, (7.2), must be equal to the rate R_e, and hence the slope at large distances from the center of the etch pit is

$$a/l = R_e/v_\infty \tag{7.13}$$

Since v_∞ is at most linear in $\Delta\mu$, the slope increases rapidly with $\Delta\mu$ in the vicinity of $\beta\Delta\mu = -0.8$. Another phenomenon observed in Fig. 18 is the presence of a steep slope close to the etch pit center. The short step segments in this region recede more slowly than the velocity v_∞. The motion of such a step segment requires a one-dimensional nucleation of a row of vacancies. The rate of nucleation and hence the average step velocity is proportional to the number of nucleation sites or the length of the step. However, when the step is long enough that several such

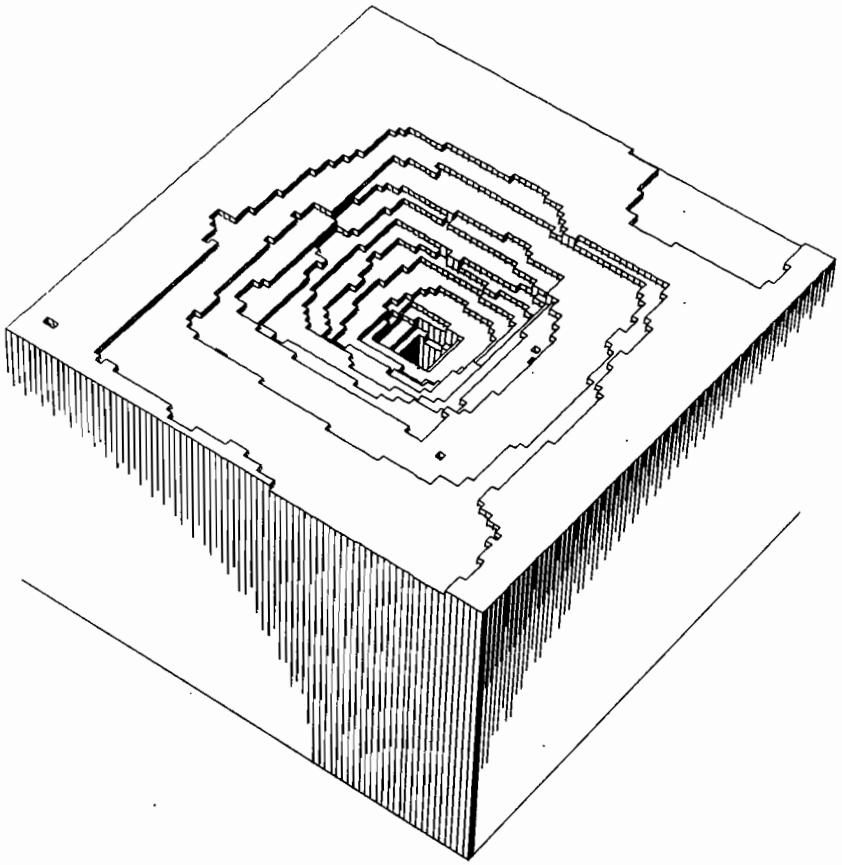

Fig. 18. Computer drawing of the etch pit formed during evaporation of a crystal containing a hole. Here $\beta\phi = 4$ and $\beta\Delta\mu = -2$.

vacancy "nuclei" are present simultaneously, the step velocity approaches a limiting value v_∞ (See Section IV for a discussion of the limiting crystal growth rate as a result of 2d nucleation.) If the dependence of the step velocity on its length were known, a generalization of (7.12) could be employed to calculate the average profile of the etch pit.

Screw dislocations also have a core region with a high concentration of strain energy. This is not included in the SOS model or the MC calculations discussed above, but the strain energy also enhances the evaporation rate. Cabrera and Levine estimated the assymmetry between growth and evaporation in their theory of the spiral mechanism. Because of the strain energy, they found that the shape of the spiral is indeterminate when the chemical potential is below a critical (negative) value. Then the atoms can

evaporate from the core region more rapidly than could be accomplished by the rotation of the spiral. Again, an etch pit with steep sides develops under these conditions.

Finally, we point out that crystal faces that are investigated in the laboratory are normally bounded by edges, that is, the intersection of the faces with other low-index faces. Atoms at these edge positions may also evaporate preferentially, and the edges can provide a ready source of steps for the evaporation process. A transient period is required before steps from the edges are distributed over an appreciable fraction of the surface. As a result, the relative importance of line defects, voids, and edges depends on the number of defects, the size of the crystal, and the length of the evaporation period. Edges are not present in the computer simulation models, since periodic boundary conditions provide lateral neighbors for these atoms.

In summary, we have seen that line defects can have different effects on the kinetics of growth and evaporation. Edge dislocations and holes affect primarily the evaporation rate. Screw dislocations enhance both processes, and they are crucial to the growth of crystals at low temperatures and driving forces. Above the roughening temperature these defects have little influence on the kinetics.

VIII. IMPURITIES

The presence of minute quantities of certain impurities can have a dramatic effect on the growth rates. Some impurities are known to act as inhibitors, but others facilitate the growth of high-quality crystals. In this section, we first consider the effect on the kinetics of small quantities of a component that bonds strongly to the crystal surface. Then we discuss the trapping of volatile impurities by the growing crystal. Impurity poisoning of the surface and step bunching have also been studied,[66] but are not included in this review.

A. Impurity-Enhanced Nucleation

The early stages of cluster formation are enhanced by the presence of impurities with strong interactions. Atoms that impinge on a site next to such an impurity have a smaller probability of evaporation than similarly coordinated atoms elsewhere. The crystal growth rates on the SC (001) face with $\phi_{AB} = 2\phi_{AA}$, and $\phi_{BB} = \phi_{AA} = 4kT$ are shown in Fig. 19. (Detailed condensation and evaporation rates with impurities are provided in Refs. 43 and 65; also see below.) Here a perfect crystal lattice is employed, and both species are immobile. Growth rates with a small quantity of impurity atoms are indicated by the triangular symbols, here

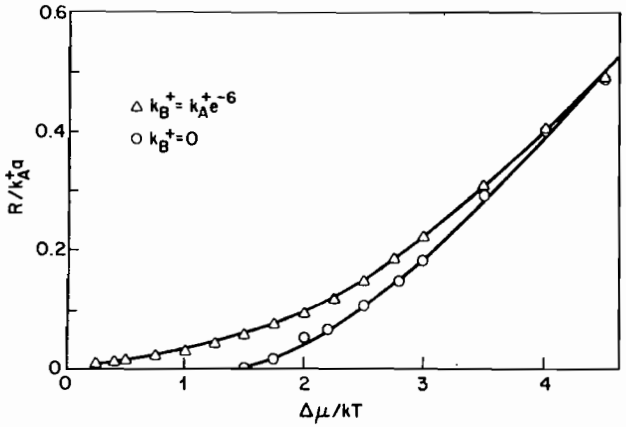

Fig. 19. Growth rates by MC calculations in a system containing impurities. Here $\beta\phi_{AB} = 8$, $\beta\phi_{AA} = 4$, $\beta\phi_{BB} = 4$, and the relative impurity impingement rates are indicated on the figure.

$\mu_B = \mu_A - 6kT$. Growth rates without impurities are plotted for comparison. Although the impingement rate of the impurity is small, a high percentage is trapped by the growing crystal because of the large AB bond energy. At small positive values of $\Delta\mu$, the nucleation of clusters occurs only around impurity atoms, and this process permits measurable growth to occur in a region where the (001) face is essentially immobile without the B atoms. The kinetics appear to be similar to those of spiral growth, except that in this case the dependence of R on $\Delta\mu$ is approximately linear at small values of $\Delta\mu$. Consequently, a break in the curve occurs near $\Delta\mu = 1.8kT$, where the nucleation rate without impurities becomes appreciable.

This type of impurity reduces the anisotropy of the growth rate with orientation. Vicinal faces and those containing weak bond networks between the atoms in the surface layer normally grow faster than close-packed faces. The anisotropy is especially large at small values of $\Delta\mu$, where the 2d nucleation rate is very slow. Since the impurities facilitate the nucleation of clusters on all types of faces, the growth rate with impurities is less sensitive to orientation. This mechanism may explain the effectiveness of certain impurities as smoothing agents for electroplated deposits on polycrystalline substrates.[67]

A crystal grown under the conditions described above and at a small positive value of $\Delta\mu$ is in a metastable condition. A large reduction in the total free energy would result from a transformation to a sodium chloride structure where each A atom is surrounded by six B nearest neighbors. The formation of the strong AB bonds would more than compensate for the lower chemical potential of the B atoms. In this case the kinetics of growth, that is, the small impingement rate of the B atoms, produces a highly nonequilibrium composition. As $\Delta\mu$ is decreased, the percentage of B atoms in the crystal increases, indicating a tendency to approach the equilibrium composition. If such a crystal remains in contact with a vapor containing B atoms at this chemical potential without growing, it will eventually transform to approximately the 1:1 stoichiometry. In practice, this process may take a very long time, since bulk diffusion rates for these impurities are usually quite low. Furthermore, in most cases the chemical potential of the impurities is even smaller than the value employed here. The value of $\Delta\mu_B$ used in the simulation was selected to induce large growth rates and short computation times, but very large increases in the growth rate also occur at much smaller concentrations.

B. Segregation of Impurities During Crystal Growth

The previous discussion concerned the effect of impurities on the growth rate. Another important aspect of this problem is the effect of the growth rate (or driving force) on the capture of impurities by the crystal. Many industrial applications involve the growth of crystals containing several different atomic species. Composition control is an important objective. For example, the concentration of dopants and the uniformity of their distribution in semiconductor crystals determine the electrical properties of the product. Here we attempt to relate the composition of the crystal to that of the fluid adjacent to the growing crystal surface. Again, we do not discuss mass transport effects in the bulk phases.

The distribution coefficient K is defined as the ratio of the atomic concentration of the impurity in the crystal to that in the fluid. This coefficient is determined by the phase diagram in the limit of an infinitesimal growth rate, since sufficiently slow growth allows time for equilibration between the phases. In the limit of a very large driving force, almost all of the atoms impinging on the surface are incorporated into the growing crystal. Then $K \cong 1$, and the composition has no relation to the phase diagram. We discuss the distribution coefficient at finite driving forces using results derived from an analytical model and from computer simulations of the simple cubic Ising model.

The capture of impurities is intimately related to the details of the crystal growth process. It has been shown that atoms impinging on all of the surface sites have an appreciable chance of being captured.[62] Even the adatoms may be trapped by an advancing step or cluster. In principle, all the surface sites also contribute to the capture of impurities, and an exact model of the process must include all the sites.

For simplicity, however, we first treat a model that employs a single

typical" site. This model can be visualized as a row of atoms at the edge of a straight step terminated by a kink site, where condensation and evaporation occur.[43,68] There is some justification for this drastic oversimplification. First, MC data indicate that a plurality of the atoms captured by the growing crystal actually impinge on kink sites (in the absence of surface migration).[62] Second, an atom in the kink site is intermediate in bonding between the various surface atoms, and we might expect it to approximate the average behavior of the system. The ultimate test of its validity is obtained when we compare this model with a corresponding MC system that is free of such restrictions.

Here we discuss the case in which the atomic concentration of impurities in the crystal is much less than unity, and impurity-impurity interactions may be neglected. Some possible positions of the impurity relative to the kink site are shown in Fig. 20. Accordingly, we define x_n as the fraction of systems in a kinetic ensemble that have an impurity located n atoms down the row from the kink site. The rate of incorporation of impurities (B atoms) at the kink site is

$$Q_B \cong k_B^+ - x_0 k_{AB}^- \tag{8.1}$$

and that for atoms of the host lattice (A atoms) is

$$Q_A \cong k_A^+ - k_{AA}^- \tag{8.2}$$

Here k_B^+ and k_A^+ are the two condensation rates, and k_{AB}^- and k_{AA}^- are the evaporation rates from "pure" kink sites, where the nearest neighbors are

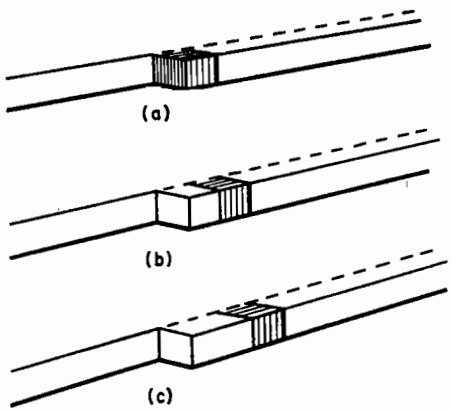

Fig. 20. An impurity atom is illustrated in various positions included in the analytical model: (a) at the kink site, (b) one unit removed, and (c) two units removed.

all A atoms. The distribution coefficient K is

$$K = (Q_B/Q_A)/(k_B^+/k_A^+) \tag{8.3}$$

but the evaluation of Q_B depends on x_0.

The probability x_0 is determined by the rates of transition between the configurations of Fig. 20. Equating the creation and annihilation rates for configuration (a), we obtain

$$k_B^- + x_1 k_{BA}^- = x_0 k^+ + x_0 k_{AB}^- \tag{8.4}$$

The terms on the left represent the rate of creation of configuration (a) by the impingement of an impurity atom at a pure kink site, and by the evaporation of an A atom from configuration (b). The terms on the right account for annihilation of (a) by the impingement of an A atom, and by the evaporation of the B atom at the kink site. The equality must be satisfied in the steady state. Similar equations apply to the other configurations, that is,

$$x_0 k_A^+ + x_2 k_{AA}^- = x_1 k_A^+ + x_1 k_{BA}^- \tag{8.5}$$

applies to (b), where k_{BA}^- is the rate of evaporation of an A atom with one B nearest neighbor. Also, for $n > 1$,

$$x_{n-1} k_A^+ + x_{n+1} k_{AA}^- = x_n k_A^+ + x_n k_{AA}^- \tag{8.6}$$

The solution to these equations is simplified if we realize that the concentration of impurity x_n must approach a constant value x_∞ for large n. Substitution in (8.6) reveals that $x_n = x_\infty$ for all $n > 0$. That is, the concentration of impurities is not a function of position except at the kink site. Substituting $x_1 = x_\infty$ and $x_2 = x_\infty$ in (8.4) and (8.5), we obtain two independent relations between x_0 and x_∞. Solving for x_0 and substituting the expressions for Q_B and Q_A into (8.3), we find

$$K^{-1} = 1 + \frac{k_{AB}^-}{k_A^+} - \frac{k_{AA}^-}{k_A^+} + \frac{k_{AB}^- k_{BA}^-}{(k_A^+)^2} - \frac{k_{AB}^- k_{AA}^-}{(k_A^+)^2} \tag{8.7}$$

Chernov first derived this equation by a different analysis.[68]

We have also calculated the impurity capture rate by the MC technique.[43] Both A and B atoms impinge on the crystal surface, but the AB bond is somewhat weaker than the AA bond. The composition of the deposit is measured, and K is determined by a comparison of this composition with the ratio k_B^+/k_A^+. In every case, k_B^+ is chosen such that the deposit contains less than 5% B atoms.

The parameters in (8.7) are readily identified in terms of the transition probabilities of the MC model. As before, the evaporation rate of an A

atom in a pure kink site is $k_{AA}^{-}=k_{A}^{+}e^{-\beta\Delta\mu}$. Then $k_{AB}^{-}=k_{A}^{+}e^{-3\beta(\phi_{AB}-\phi_{AA})-\beta\Delta\mu}$. That is, we assume that the difference between the two rates is determined entirely by the fact that three AA bonds are replaced by AB bonds. For simplicity we assume that preexponential factors are identical. Similarly, $k_{BA}^{-}=k_{A}^{+}e^{-\beta(\phi_{AB}-\phi_{AA})-\beta\Delta\mu}$.

A comparison of the two models is presented in Fig. 21.[43] MC data for a stepped plane are represented by the open circles, triangles, and squares for $\phi_{AB}=3.5kT$, $3kT$, and $2.25kT$, respectively. In all cases $\phi_{AA}=4kT$. The agreement with the analytical model (dashed lines) is quite good, considering the simplicity of the approach. The discrepancies at both ends of the range of $\Delta\mu$ are expected. When $\Delta\mu\to 0$, the MC data must approach the true bulk equilibrium coefficient $K_{eq}=e^{6\beta(\phi_{AB}-\phi_{AA})}$, and the solid curves were constructed to intersect the axis at this point. The dashed curves of (8.7) intersect the axis at a larger value, $K_{eq}^{s}=e^{4\beta(\phi_{AB}-\phi_{AA})}$, the equilibrium value for the edge of a step. This is inherent in the model, and the inclusion of the other processes that result in the complete immuring of the impurity is necessary to obtain K_{eq}. At very large $\Delta\mu$, (8.7) also predicts a larger value of K than the MC data. Impurity atoms landing at sites with only one or two bonds to the crystal

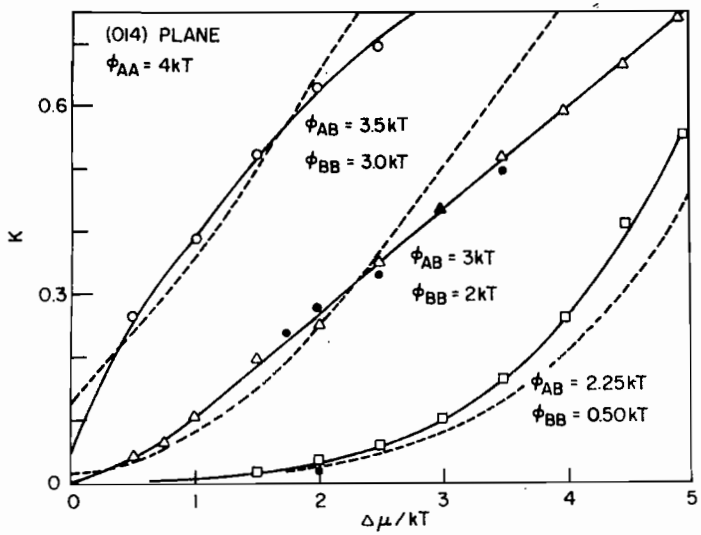

Fig. 21. The distribution coefficient K is plotted as a function of the driving force. Data for three different values of the impurity-host bond energy are illustrated. The solid curves and open symbols are MC data taken on a stepped (041) surface, and the dashed curves correspond to Eq. (8.7). The solid circles are MC data taken on a (001) surface.

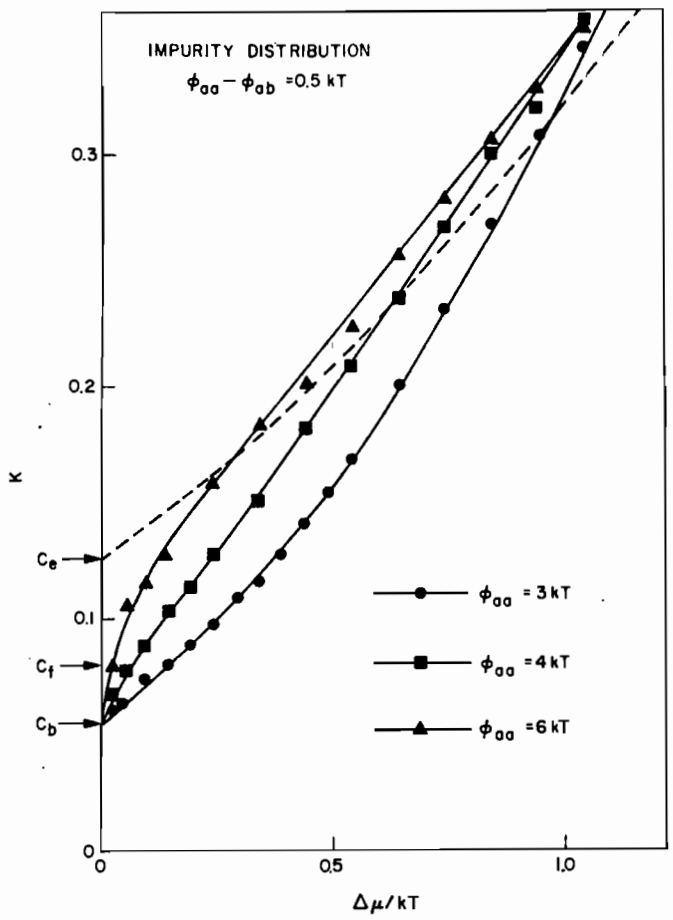

Fig. 22. The distribution coefficient with relatively small values of the driving force.

are rejected with a much higher probability than those landing at kink sites. The nonlinear nature of the exponential function causes the "typical site" rate to deviate from the average rate of the MC model.

The effect of crystallographic orientation on the distribution coefficient was also examined. Values of K at the (001) orientation are indicated by the small black dots. These data are limited to the larger values of $\Delta\mu$ because of the small 2d nucleation rate otherwise. The close agreement between these two sets of data implies that the distribution coefficient is determined primarily by $\Delta\mu$.

Accurate MC data at small values of $\Delta\mu$ are shown in Fig. 22. (The

square symbols correspond to the data with $\phi_{AA} = 3.5kT$ in Fig. 21.) The composition approaches the bulk equilibrium value as $\Delta\mu \to 0$. Note that the value of $\beta\phi_{AA}$ affects the composition at small values of $\Delta\mu$, although this parameter does not appear in (8.7). The evaporation of impurities from sites with four or five bonds to the crystal is not included in the analytical model, but these processes are important at small driving force and permit the reduction of the impurity concentration below the value captured by the kink sites. At the smaller values of ϕ_{AA} these processes occur more frequently, and the lowest values of the impurity concentrations are obtained.

The weak dependence of K on orientation affords an explanation of the enhanced impurity concentration at facets. This enhancement is observed in crystals grown by the Czochralski method.[69] The steady-state pulling of a crystal from the melt imposes a constant average growth rate over the entire surface. Except for temporal fluctuations, the center of the facet and the vicinal orientations have growth rates that are nearly identical. A much greater driving force is required at the center of the facet, since 2d nucleation is necessary. This larger driving force then induces a larger value of K. This effect is observed for a large number of impurities in germanium and silicon.

It is evident that surface mobility can cause a drastic change in K. For example, an impurity with a relatively high surface mobility may exhibit a value of K greater than unity, even when $\phi_{AB} < \phi_{AA}$. This has been demonstrated by MC simulations.[25] Rapid surface diffusion allows impurity atoms to migrate to sites where they are strongly bonded to the crystal. We noted in the preceding section the large increase in growth rate (or capture probability) that occurs when surface mobility is included. In some cases this can more than compensate for the weaker bonding of the impurity to the crystal.

In summary, the primary factors that determine the distribution of impurities in a growing crystal are (*1*) the driving force $\Delta\mu$ prevailing in the interfacial region, (*2*) the relative surface mobility of the impurity and host atoms, and (*3*) the interaction energies ϕ_{AA}, and ϕ_{AB}. The crystal surface orientation and crystalline perfection may, in some circumstances, determine the magnitude of the driving force. In these cases they affect the composition indirectly through the driving force.

IX. FINAL REMARKS

In this article we have reviewed theories and computer simulation results for crystal growth using the kinetic SOS model. We seem to have a good theoretical understanding of growth on close-packed faces of perfect crystals that are free of impurities. Theories for the low temperature nucleation regime and the high temperature continuous growth regime are in good agreement with the MC data. Recent work has also greatly advanced our knowledge of the nature of the roughening transition between these two regimes.

We have concentrated on the properties of the SC (001) face on the assumption that it is typical of close-packed surfaces in general. Although we expect universal behavior in the vicinity of the roughening temperature, the absolute magnitude of T_R depends on the details of the atomic interactions and the geometrical arrangement of atoms in the close-packed plane. It has been found in the case of the SOS model that the roughening temperature is slightly greater than the critical temperature of the 2d array of surface atoms. This has been verified in the case of the SC (001) face (Section V) and for the FCC (001) and (111) faces.[43,70] Calculations of T_R for other systems would be very helpful, especially in the case when continuous atomic coordinates are permitted. It is important to determine the degree of localization of atoms in the vicinity of lattice sites at the transition temperature. Molecular dynamics simulations will undoubtedly play an important role in these studies.

Monte Carlo simulations have provided a powerful method for assessing the contribution of defects and impurities to the motion of the interface. The simulations show that often several mechanisms operate in parallel, and the resulting kinetics may not agree with existing theories that assume idealized and simplified conditions. The theories are usually in agreement with MC data on systems that are constrained to permit only a single growth mode (e.g., spiral growth), but there may be large discrepancies between the same theories and MC data on more realistic systems without such constraints.

The development of theories that apply to very general conditions is a goal for the future. It is important to have analytic theories to help clarify the physics of the various processes, to facilitate comparison with experimental data, and to suggest new effects. Existing MC data provide definitive results against which the theories can be tested and improved.

Another important aspect of crystal growth requiring further study is the stability of an array of steps on the crystal surface. The kinetic repulsion mentioned briefly in Section VII has a stabilizing effect on the array, but impurities[66] or the anisotropic capture of migrating atoms[71–73] may have the opposite effect. That is, an instability that leads to step bunching may occur because of impurities or because of the kinetics of surface migration. Relatively steep macrosteps (step bunches) separated

by low-index terraces are commonly observed on crystals that have been grown from the vapor and from solution.[74] The theory of the stability of arrays of steps is in a very primitive state.

Improvements in the basic kinetic SOS model are also needed for a more realistic description of the experimental situation. Models that allow continuous coordinates and can consider effects such as strain energy and impurity size effects represent an important area for future work. These improvements are particularly needed for an accurate description of melt growth. Also, the connection between the microscopic approach taken here and macroscopic effects of bulk transport and such questions as morphological stability need clarification.

The theory of crystal growth offers a host of challenging problems of great practical importance. As this article makes clear, we are now beginning to deal with some of the complicated effects that arise in the laboratory, but much work remains to be done. We believe it represents a fruitful area of research for some time to come.

Acknowledgments

Part of the work reviewed herein was done in collaboration with S. T. Chui, K. A. Jackson, and H. J. Leamy. Without their contributions, it would not have been possible to write this review. We are also grateful to P. C. Hohenberg for many helpful and patient discussions.

References

1. R. F. Sekerka, in *Crystal Growth: An Introduction*, North-Holland, Amsterdam, 1973, p. 403.
2. See, for example, K. Huang, *Statistical Mechanics*, Wiley, New York, 1963, p. 329.
3. K. A. Jackson, in *Liquid Metals and Solidification*, American Society for Metals, Metals Park, Ohio, 1958, p. 174.
4. D. E. Temkin, in *Crystallization Processes*, Consultants Bureau, New York, 1966, p. 15.
5. F. F. Abraham and G. H. White, *J. Appl. Phys.*, **41,** 1841 (1970).
6. G. H. Gilmer, *J. Crystal Growth*, **35,** 15 (1976).
7. R. Becker and W. Doering, *Ann. Physick*, **24,** 719 (1935).
8. W. K. Burton, N. Cabrera, and F. C. Frank, *Phil. Trans. R. Soc* (London), **243A,** 299 (1951).
9. H. J. Leamy, G. H. Gilmer, and K. A. Jackson, in J. B. Blakeley, ed., *Surface Physics of Materials I*, Academic Press, New York, 1975. Also see: W. J. Shugard, J. D. Weeks, and G. H. Gilmer, *Phys. Rev. Lett.* **41,** 1399 (1978).
10. S. T. Chui and J. D. Weeks, *Phys. Rev.*, **B14,** 4978 (1976).
11. H. Van Beijeren, *Phys. Rev. Lett.*, **38,** 993 (1977).
12. H. J. F. Knops, *Phys. Rev. Lett.*, **39,** 776 (1977).
13. H. J. Leamy and G. H. Gilmer, *J. Crystal Growth*, **24/25,** 499 (1974).
14. R. H. Swendsen, *Phys. Rev.*, **B15,** 5421 (1977).
15. H. P. Bonzel, in J. B. Blakeley, ed., *Surface Physics of Materials*, Academic Press, New York, 1975.
16. J. D. Weeks, G. H. Gilmer, and K. A. Jackson, *J. Chem. Phys.*, **65,** 712 (1976).

17. The limiting growth law for melt growth was derived by H. A. Wilson, *Philos. Mag.*, **50,** 238 (1900) and by J. Frenkel, *Phys. Z. Sowjetunion*, **1,** 498 (1932). The corresponding limiting law for growth from the vapor phase is due to H. Hertz, *Ann. Phys.* (*Leipzig*), **17,** 177 (1882) and M. Knudsen, *Ann. Phys.* (*Leipzig*), **29,** 179 (1909). J. W. Gibbs, *Collected Works*, Yale University, New Haven, 1957, p. 325 footnote, realized the limitations imposed on growth by the formation of new layers of a crystal. W. Kossel, *Nachr. Ges. Wiss. Göttingen*, **135,** (1927); I. N. Stranski, *Z. Phys. Chem Leipzig*, **136,** 259 (1928); and J. Frenkel, *J. Phys. USSR*, **9,** 302 (1945) discussed the importance of steps and kink sites in crystal growth.
18. D. E. Temkin, *Soviet Phys. Crystallogr.*, **14,** 344 (1969).
19. D. Walton, *J. Chem. Phys.*, **37,** 2182 (1962).
20. G. H. Gilmer, in *Computer Simulation for Materials Applications*, National Bureau of Standards, Gaithersburg, Md. 1976, p. 964.
21. J. J. Burton, in B. J. Berne, ed., *Statistical Mechanics, Part A*, Plenum, New York, 1977.
22. G. H. Gilmer and J. D. Weeks, *J. Chem. Phys.*, **68,** 950 (1978).
23. C. van Leeuwen and P. Bennema, *Surf. Sci.*, **51,** 109 (1975).
24. A. E. Michaels, G. M. Pound, and F. F. Abraham, *J. Appl. Phys.*, **45,** 9 (1974).
25. G. H. Gilmer, unpublished.
26. A. E. Nielsen, *Kinetics of Precipitation*, Pergamon, Oxford, 1964.
27. E. Budevski, V. Bostanov, T. Vitanov, Z. Stoynov, A. Kotzeva, and R. Kaischev, *Phys. Status Solidi*, **13,** 577 (1966); *Electrochim. Acta*, **11,** 1697 (1966).
28. A. N. Kolmogorov, *Izv. Akad. Nauk Ser. Math.*, No. 3, 355 (1937).
29. W. B. Hillig, *Acta Met.*, **14,** 1968 (1966).
30. S. K. Rangarajan, *J. Electroanalyt. Chem.*, **46,** 125 (1973).
31. L. A. Borovinskii and A. N. Tsindergozen, *Sov. Phys. Crystallography*, **13,** 1191 (1969).
32. M. Hayashi, *J. Phys. Soc. Jap.*, **35,** 614 (1974).
33. U. Bertocci, *Surf. Sci.*, **15,** 286 (1969).
34. J. W. Oldfield, *Electrodeposition and Surf Treatment*, **2,** 395 (1973/74).
35. V. Bostanov, R. Roussinova, and E. Budevski, *J. Electrochem. Soc.*, **119,** 1346 (1972).
36. See, for example, Ref. 2, Chap. 16.
37. H. van Beijeren, *Commun. Math. Phys.*, **40,** 1 (1975).
38. K. A. Jackson, *J. Crystal Growth*, **3/4,** 507 (1968).
39. K. A. Jackson, in *Crystal Growth*, Pergamon, New York, 1967, p. 17.
40. J. D. Weeks, G. H. Gilmer, and H. J. Leamy, *Phys. Rev. Lett.*, **31,** 549 (1973).
41. G. H. Gilmer, K. A. Jackson, H. J. Leamy, and J. D. Weeks, *J. Phys.*, **C7,** L123 (1974).
42. See, for example, J. W. Essam, and M. E. Fisher, *J. Chem. Phys.*, **38,** 8021 (1963) for a good discussion of low temperature series analysis.
43. G. H. Gilmer and K. A. Jackson, in *Crystal Growth and Materials*, North-Holland, Amsterdam, 1977, p. 79.
44. J. M. Kosterlitz, *J. Phys.*, **C7,** 1046 (1974). See also J. M. Kosterlitz and D. J. Thouless, *J. Phys.*, **C6,** 1181 (1973). The method was used earlier for the Kondo problem by P. W. Anderson and G. Yuval, *J. Phys.*, **C4,** 607 (1971).
45. J. V. José, L. P. Kadanoff, S. Kirkpatrick, and D. R. Nelson, *Phys. Rev.*, **B16,** 1217 (1977).
46. E. H. Lieb, *Phys Rev. Lett.*, **18,** 692, 1046 (1967); E. H. Lieb and F. Y. Wu, in C. Domb and M. S. Green, eds., *Phase Transitions and Critical Phenomena*, vol. 1, Academic Press, London, 1972.
47. R. H. Swendsen, *Phys. Rev.*, **B17,** 3710 (1978).
48. S. T. Chui and J. D. Weeks, *Phys. Rev. Lett.*, **40,** 733 (1978).

49. For a general introduction to critical phenomena (including critical dynamics) see S. K. Ma, *Modern Theory of Critical Phenomena*, W. A. Benjamin, Reading, Mass., 1976.
50. B. I. Halperin, P. C. Hohenberg, and S. Ma, *Phys. Rev. Lett.*, **29,** 1548 (1972).
51. P. C. Hohenberg and B. I. Halperin, *Rev. Mod. Phys.*, **49,** 435 (1977).
52. P. G. de Gennes, *Faraday Symposium #5 on Liquid Crystals*, London, 1971, p. 16.
53. See for example, Ref. 49, Chaps. XI–XIV.
54. D. R. Nelson and J. M. Kosterlitz, *Phys. Rev. Lett.*, **39,** 1201 (1977).
55. M. Volmer and W. Schultz, *Z. Phys. Chem.*, **A156,** 1 (1931).
56. F. C. Frank, *Disc. Faraday Soc.*, **5,** 48 (1949).
57. E. E. Gruber and W. W. Mullins, *J. Phys. Chem. Solids*, **28,** 875 (1967).
58. E. Budevski, G. Staikov, and U. Bostanov, *J. Crystal Growth*, **29,** 316 (1975).
59. R. H. Swendsen, P. S. Kortman, D. P. Landau, and H. Müller-Krumbhaar, *J. Crystal Growth*, **35,** 73 (1976).
60. N. Cabrera and M. M. Levine, *Phil. Mag.*, **1,** 450 (1956).
61. N. Cabrera and R. V. Coleman, in J. J. Gilman, ed., *The Art and Science of Growing Crystals*, Wiley, New York, 1963, p. 3.
62. G. H. Gilmer and P. Bennema, *J. Appl. Phys.*, **43,** 1347 (1972).
63. H. T. Minden, *J. Crystal Growth*, **8,** 37 (1971).
64. T. Surek, J. P. Hirth, and G. M. Pound, *J. Crystal Growth*, **18,** 20 (1973).
65. G. H. Gilmer, *J. Crystal Growth*, **42,** 3 (1977).
66. F. C. Frank, in *Growth and Perfection of Crystals*, Wiley, New York, 1958, p. 411.
67. J. D. E. McIntyre and W. F. Peck, Jr., *J. Electrochem. Soc.*, **123,** 1800 (1976).
68. A. A. Chernov, *Sov. Phys.-Uspekhi*, **13,** 101 (1970).
69. J. A. M. Dickhoff, *Solid State Electron*, **1,** 202 (1960).
70. U. Bertocci, *J. Crystal Growth*, **26,** 219 (1974).
71. R. L. Schwoebel, *J. Appl. Phys.*, **40,** 614 (1969).
72. R. Ghez and G. H. Gilmer, *J. Crystal Growth*, **21,** 93 (1974).
73. C. van Leeuwen, R. van Rosmalen, and P. Bennema, *Surf. Sci.*, **42,** 32 (1974).
74. D. L. Rode, *J. Crystal Growth*, **27,** 313 (1974).